AD-A013 321

UV GAS LASER INVESTIGATIONS

E. R. Ault, et al

Northrop Research and Technology Center

Prepared for:

Office of Naval Research
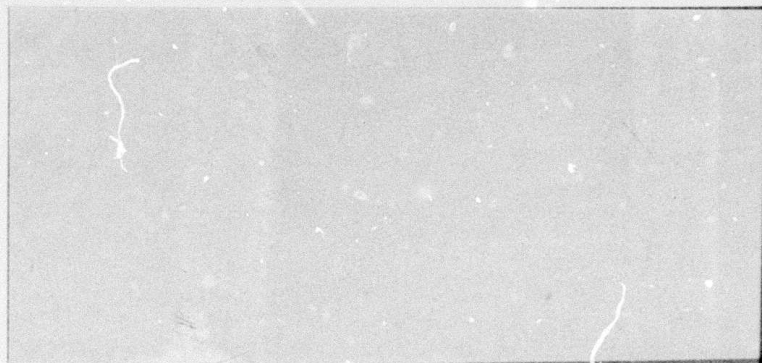Advanced Research Projects Agency

May 1975

ADA013321

230097

D D C
RECEIVED
AUG 8 1975
A

NORTHROP
Research and Technology Center

REPORT DOCUMENTATION PAGE		READ INSTRUCTIONS BEFORE COMPLETING FORM
1. REPORT NUMBER NRTC 75-28R	2. GOVT ACCESSION NO.	3. RECIPIENT'S CATALOG NUMBER
4. TITLE (and Subtitle) UV Gas Laser Investigations		5. TYPE OF REPORT & PERIOD COVERED Semiannual Technical Report 1 Nov. 1974-30 April 1975
		6. PERFORMING ORG. REPORT NUMBER NRTC 75-28R
7. AUTHOR(s) E. R. Ault, R. S. Bradford, Jr., and M. L. Bhaumik		8. CONTRACT OR GRANT NUMBER(s) N00014-72-C-0456
9. PERFORMING ORGANIZATION NAME AND ADDRESS Northrop Research and Technology Center 3401 West Broadway Hawthorne, California 90250		10. PROGRAM ELEMENT, PROJECT, TASK AREA & WORK UNIT NUMBERS ARPA Order No. 1807
11. CONTROLLING OFFICE NAME AND ADDRESS Advanced Research Projects Agency 1400 Wilson Blvd. Arlington, Virginia 22209		12. REPORT DATE May 1975
		13. NUMBER OF PAGES 52
14. MONITORING AGENCY NAME & ADDRESS(If different from Controlling Office) Office of Naval Research Department of the Navy Arlington, Virginia 22217		15. SECURITY CLASS. (of this report) Unclassified
		15a. DECLASSIFICATION/DOWNGRADING SCHEDULE -

16. DISTRIBUTION STATEMENT (of this Report)

DISTRIBUTION STATEMENT A

Approved for public release;
Distribution Unlimited

17. DISTRIBUTION STATEMENT (of the abstract entered in Block 20, if different from Report)

None

18. SUPPLEMENTARY NOTES

None

19. KEY WORDS (Continue on reverse side if necessary and identify by block number)

Laser Oscillations
$Ar-N_2$
Transfer Lasers
Ultraviolet Lasers
High Power Xenon Lasers

20. ABSTRACT (Continue on reverse side if necessary and identify by block number)

The development of the first table-top E-beam excited laser and the quasi-cw operation of the $Ar-N_2$ laser with an output pulse of 150 ns is described. Using the table-top E-gun, an output energy of 125 mJ was extracted from a 100 cm^3 $Ar-N_2$ laser with an overall efficiency of 0.05%. Peak laser powers of 10 MW and 400 MW were also obtained in a 25 ns pulse from $Ar-N_2$ and Xe, respectively, using the Physics International Pulserad 535 E-gun.

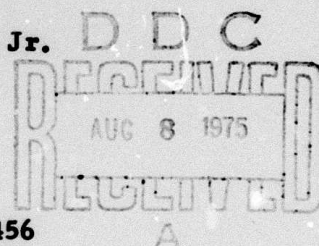DD FORM 1473 1 JAN 73   EDITION OF 1 NOV 65 IS OBSOLETE

UV GAS LASER INVESTIGATIONS

SEMIANNUAL TECHNICAL REPORT

May 1975

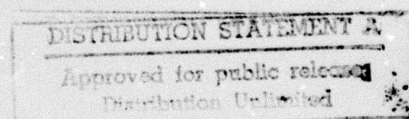Prepared by

E. R. Ault, R. S. Bradford, Jr.
and M. L. Bhaumik

Contract N00014-72-C-0456

Sponsored by

ADVANCED RESEARCH PROJECTS AGENCY
ARPA Order No. 1807

Monitored by

OFFICE OF NAVAL RESEARCH
Code 421

NORTHROP CORPORATION
Northrop Research and Technology Center
Short Wavelength Laser Programs
3401 West Broadway
Hawthorne, California 90250
(213) 970-4756

UV GAS LASER INVESTIGATIONS

ARPA Order Number: 1807

Program Code Number: 5E20

Contract Number: N00014-72-C-0456

Principal Investigator   Dr. M. L. Bhaumik
and Telephone Number: (213) 970-4756

Name of Contractor: Northrop Corporation
                               Northrop Research and
                                   Technology Center

Scientific Officer: Director, Physics Programs
                               Physical Sciences Division
                               Office of Naval Research
                               Department of the Navy
                               800 North Quincy Street
                               Arlington, Virginia 22217

Effective Date of Contract: 15 April 1972 to 30 June 1975

Amount of Contract: $652,500.00

Sponsored By: Advanced Research Projects Agency
                               ARPA Order No. 1807

Reproduction in whole or in part is permitted for any purpose of the United States Government.

Disclaimer: The views and conclusions contained in this document are those of the authors and should not be interpreted as necessarily representing the official policies, either expressed or implied, of the Advanced Research Projects Agency or the United States Government.

TABLE OF CONTENTS

1.0 SUMMARY

The overall objective of this program is the development of new, visible and shorter wavelength lasers capable of high power operation with high efficiency. The specific objective for this reporting period has been to carry out analytical and experimental investigations of the $Ar-N_2$ excitation transfer laser as well as the xenon excimer laser, leading to an optimization of power and efficiency. Working toward these objectives, the following key results were obtained:

(1) A significant achievement was the demonstration of the first table-top E-beam excited $Ar-N_2$ laser. This laser was developed by successfully combining an efficient pumping scheme with a compact E-gun. A peak power of 1 MW with an efficiency of 3% was achieved in this laser using a 1.4 atm $Ar-N_2$ mixture containing 5% N_2.

(2) A quasi-cw operation of the $Ar-N_2$ laser was demonstrated by obtaining a 150 ns laser pulse which nearly followed the excitation current pulse. Under the optimum operating conditions, a maximum laser energy of 130 mJ was extracted with an overall electrical efficiency of 0.05%. This is the highest overall efficiency reported so far for E-beam excited lasers.

(3) The small signal gain coefficient and the saturation intensity of the $Ar-N_2$ laser were measured by employing a novel technique. A gain coefficient of 25% and saturation intensity of 100 kW/cm^2 were measured for a 3 atm. $Ar-N_2$ mixture with 5% N_2. A theoretical value was also obtained for the gain coefficient by kinetic modeling.

(4) Attempts were made to excite the $Ar-N_2$ laser by an overvoltaged E-beam stabilized sustainer discharge. Although pre-

1

liminary results look encouraging, laser emission was not ob-
served probably due to the large impedence of the sustainer
supply.

(5)   With partial support from the Defense Nuclear Agency, a high
power, high efficiency operation of the xenon excimer laser was
demonstrated.   A peak power in excess of 400 MW with an
efficiency of 6% was achieved on the basis of energy deposition
into the gas.   This is the highest power and efficiency reported
so far in the VUV region.

2.0   INTRODUCTION

The achievement of high efficiency vacuum ultraviolet excimer lasers has demonstrated the importance of rare gases for efficiently converting electrical energy into radiation at short wavelengths.   Analytical investigations at Northrop and other laboratories   indicate that due to uniquely favorable kinetic processes, the rare gas excimers may be capable of electrical conversion efficiencies up to 50%.   However, the radiation from the rare gas excimers occurs only in the VUV region of the spectrum.   Although high energy lasers in these wavelengths are important for some special applications, it would be more desirable to obtain high efficiency lasers in the transmissive region of the atmosphere, since that would lead to more versatile applications.

The high conversion efficiency of the rare gas excimers may be successfully employed to develop visible and near UV lasers by using suitable energy transfer schemes.   In such a scheme, the rate of energy transfer to the acceptor molecule must be higher than the rate of energy losses in the rare gas itself.   Furthermore, the branching ratio of the transferred energy to the various levels of the acceptor molecule must be favorable for a population inversion.   If a donor-acceptor pair of this type is found, which shows a high rate of energy transfer that specifically populates the upper laser level, an efficiency of 10 to 20% may be realized near visible wavelengths. A block diagram of this scheme is shown in Figure 1.

The validity of this approach was demonstrated successfully at Northrop by the operation of a high power Ar-N_2 transfer laser at 3577Å.   The pertinent energy level diagram of this system is shown in Figure 2.   In this system, electrical energy absorbed by Ar is transferred to the N_2 molecule leading to laser oscillations on the transition $C^3\Pi_u \rightarrow B^3\Pi_g$.   A peak laser power of several megawatts with an estimated efficiency of 2% was achieved by E-beam excitation of a mixture of Ar and N_2.   The details of these studies were
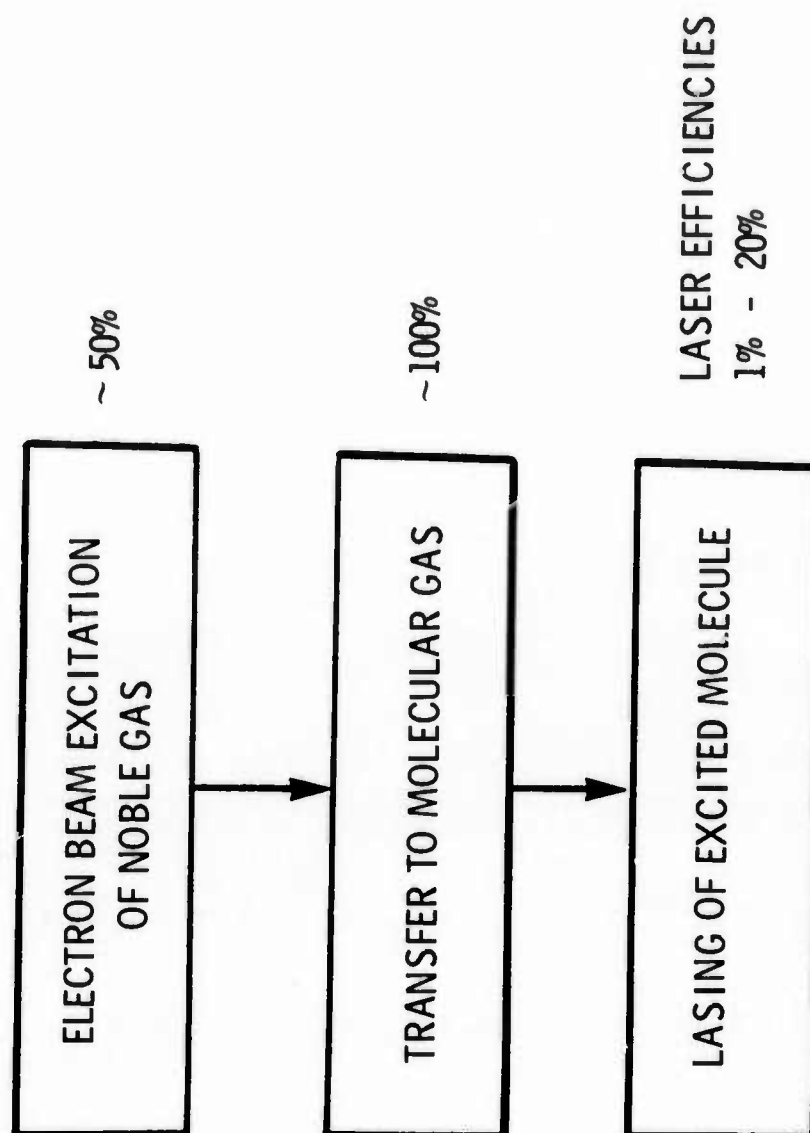
3

Figure 1. Block diagram showing our approach for developing a high efficiency laser near visible wavelengths.
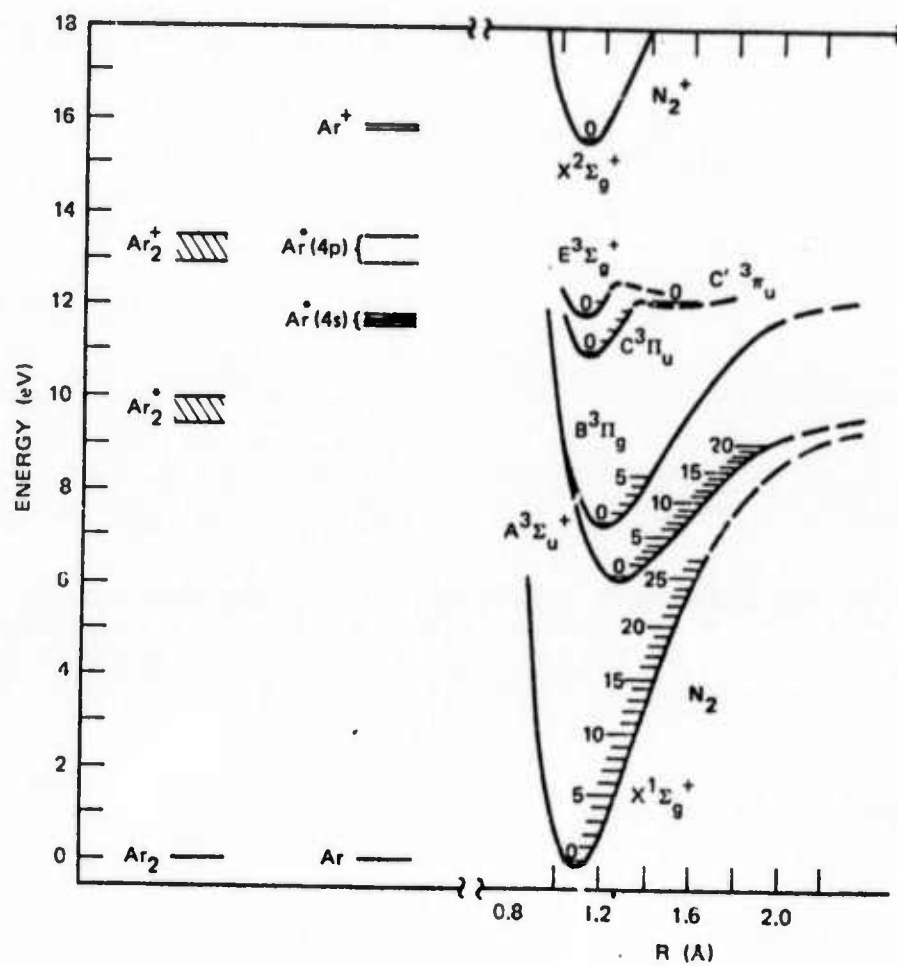
Figure 2. Pertinent energy level diagram of the Ar/N₂ system (from SRI Report MP 74-39 (1974)).

described in the previous semiannual technical reports, NRTC 74-26R and NRTC 74-70R.

The $Ar-N_2$ system deserves a thorough investigation in view of the initial success. Accordingly, a concerted effort has been devoted to the understanding of the laser mechanism by kinetic modeling and parametric investigations such as small signal gain measurements. The experimental program includes the optimization of power and efficiency of the $Ar-N_2$ laser as well as the xenon excimer laser. Progress in the program for the past six months is described in the following sections.

3.0 ACCOMPLISHMENTS DURING THE REPORTING PERIOD

The major achievements during the reporting period included the development of the first table-top E-beam excited laser and the quasi-cw operation of the Ar-N$_2$ laser. Progress was also made in understanding the Ar-N$_2$ laser mechanics by the measurement of small signal gain coefficient and saturation intensity and comparing the results of these measurements with those obtained by kinetic modeling studies. A high power, high efficiency xenon laser was also operated with an output of 10 J in a 25 ns pulse with an efficiency of 6%.

3.1 Table-Top E-Beam Excited Laser

Ultraviolet and visible lasers which utilize high pressure gases excited by relativistic electron beams show the promise of not only high quantum efficiencies, but also of high extraction efficiencies. However, to achieve this, the electrons must be effectively coupled to the laser gas. Previous electron sources have been poorly matched to the laser because of the rather long range of the relativistic beam and the use of inefficient transverse pumping geometries. This leads to the need for large electrical storage and pulse shaping networks. Because of the high currents required in this case ($> 100 A/cm^2$), the electron gun has a low impedance and requires a transmission line pulser.

This section describes our successful development of a table-top sized, coaxially excited Ar-N$_2$ transfer laser which delivered 12 mJ of energy at 3577Å in a 20 ns pulse; the output is comparable to the output energy of the Ar-N$_2$ laser obtained previously with the Pulserad 110A, a much larger electron source. With a 5% mixture of nitrogen in argon at 1.7 atm pressure, laser pulses of 300 kW with pulse widths of 40 ns FWHM were obtained. This corresponds to an energy extraction of 0.2 J/liter. The repetition rate was 1 Hz. Electrons were directed radially into a cylindrical gas cell located at the center of an annular cathode shell containing razor blade type emitters. This arrangement

has the advantage of using the radial focusing inherent in the cylindrical geometry to help overcome the beam scattering introduced by the foil and laser gas. With the coaxial design, the electron energy is deposited more effectively in the laser gas and the total stored energy required to provide the same laser output is greatly reduced.

Figure 3 shows the schematic of the coaxially excited E-beam laser. The laser gas celled consisted of an unsupported titanium foil cylinder 2.5 cm in diameter and 20 cm long with a wall thickness of 1.3×10^{-3} cm. Six longitudinal titanium foil blades were placed on the inside surface of an 8 cm inside diameter cathode shell that was concentric with the foil gas cell, the anode. Each blade was 0.5 cm wide, giving a minimum anode-cathode spacing of 2 cm. A 12-stage Marx bank was used to drive the cathode directly with a total circuit inductance of approximately 1 microhenry. Each stage of the Marx was charged to 45 kV, giving a total voltage of 450 kV. The total stored energy in the Marx was 45 J. Because of the circuit inductance, the peak cathode voltage estimated with a voltage divider at the cathode was approximately 300 kV.

A total cathode current of 3 kA was measured with an integrating magnetic pickup loop. With the gas cell (anode cylinder) evacuated, a small Faraday cup was used to probe the current transmitted by the anode foil. With a 1.3×10^{-3} cm thick foil an average of less than 8 A/cm^2 was observed over the interior of the gas cell. The current density varied by a factor of 2 as the Faraday cup was rotated just beneath the cathode blades to a location between the blades. A 4 meter radius of curvature dielectric total reflector (99.5%) and a partially transmitting output coupler formed the optical cavity. The temporal behavior of the laser and fluorescence emissions were observed with a fast planar photodiode and the laser energy measurements were made with an integrating pyroelectric joule meter.
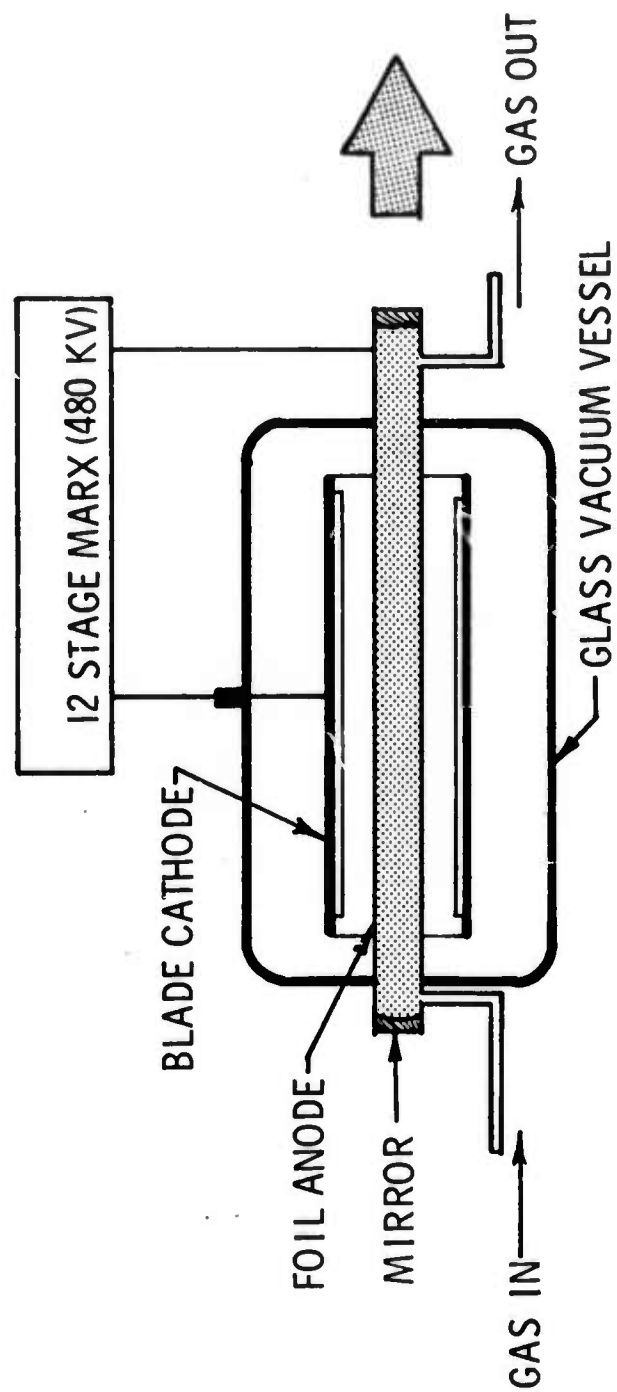
Figure 3.   Schematic of the coaxial electron gun and laser components.

9

Fluorescence measurements were made with the calibrated photodiode and calibrated neutral density filters. Having both the total reflector and the output mirror replaced with quartz windows, no superradiant emission was observed over a pressure range of 1 to 5 atm. The three transitions 3371Å, 3577Å, and 3805Å, were all seen in fluorescence. The total fluorescence peak power at 2 atm was approximately 200 watts for all three wavelengths combined. When the resonator was installed, strong laser oscillations were observed at 3577Å. The optimum pressure was found to be 1.7 atm with a mixture of 5% N_2 in argon. The maximum energy that could be extracted from the laser, using the optimum coupler and a 1.3×10^{-3} cm thick anode foil, was 12 mJ.

Figure 4 shows photodiode measurements of the laser pulse shape compared to a vacuum Faraday cup measurement of the current density taken on a previous shot. The peak power of the pulse is 300 kW. It is worthy of note that the laser pulse is nearly square topped and follows the current pulse. This leads to the speculation that the laser may be approaching a quasi-cw state. (The laser pulse has been increased subsequently to 150 ns; this is described in the next section.)

In Figure 5 the output energy is plotted against the reflectance of the output mirror. These data were taken with the more rugged 2.54×10^{-3} cm thick anode and a 10% mixture of N_2 in argon. The laser characteristics were found to vary little between 5% and 10% mixtures. A beam divergence of 4 mR was determined by measuring the increase in the laser spot diamter at a distance of 3 meters and 5 meters from the output mirror.

An estimate of the laser efficiency can be made based on the energy deposition tables published by Berger and Seltzer.[1] For the conditions of this experiment, the gas has a stopping power of 5.0 kV/cm. Integrating around the

300 KW   LASER POWER

FARADAY CUP
($\sim$10A/cm^2 PEAK)
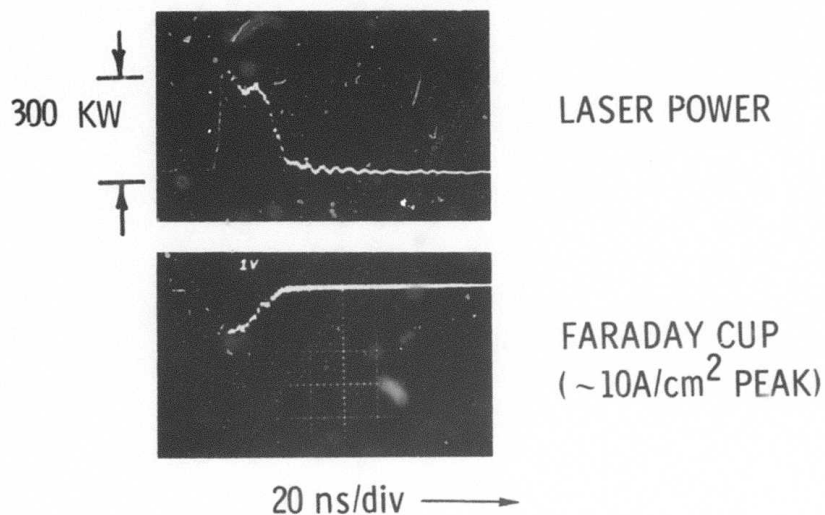
20 ns/div $\longrightarrow$

Figure 4.   Oscilloscope traces of (a) the laser power
(300 kW peak) detected by a fast planar
photodiode, and (b) the corresponding
current pulse obtained with a vacuum
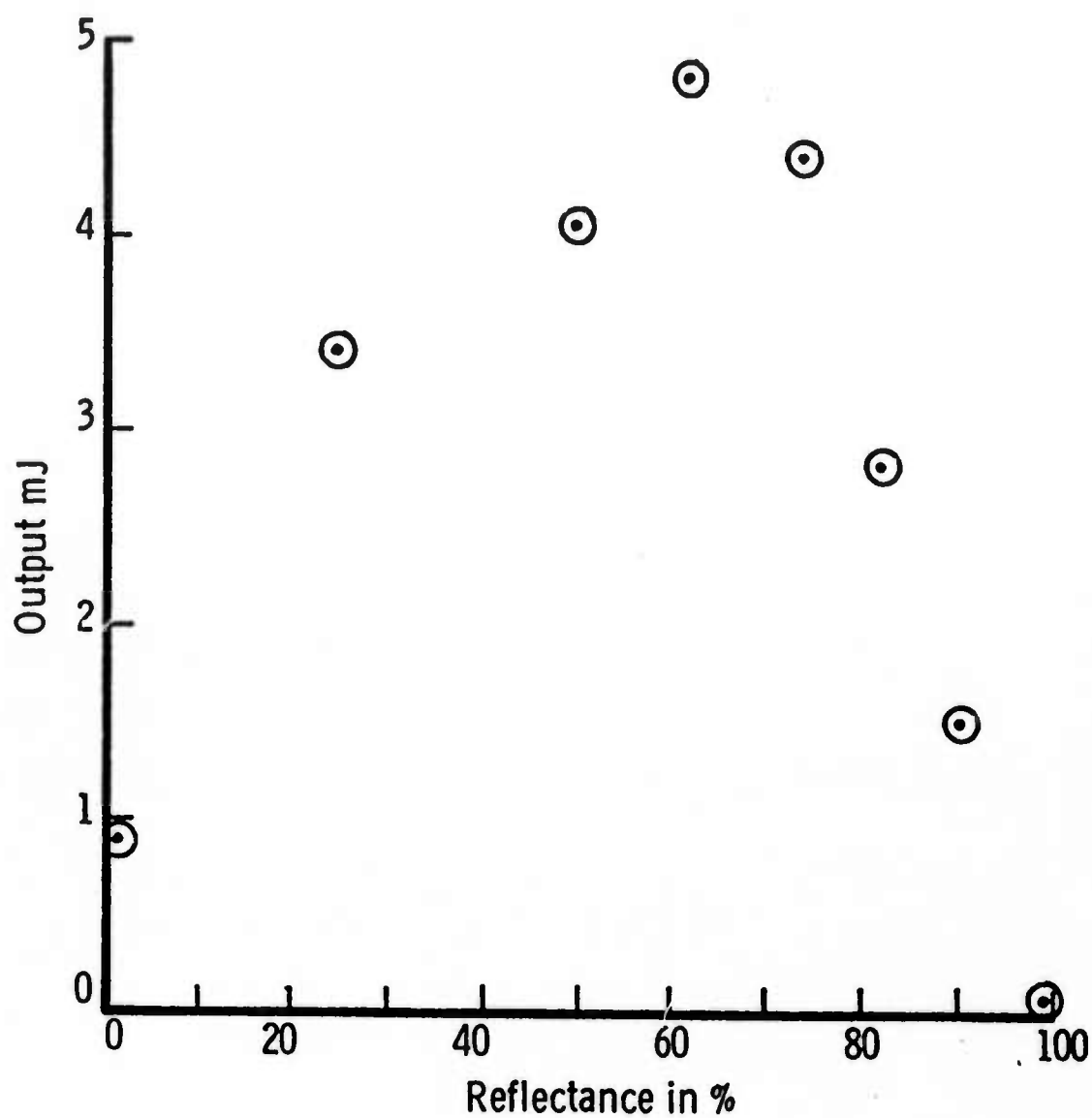Faraday cup inside the gas cell on a previous
shot.

Figure 5. The laser output energy as a function of the output mirror reflectance. A 10% mixture of N_2 in argon and a 2.5×10^{-3} cm thick anode foil were used to obtain these data.

cylindrical volume of the anode gas cell and assuming the radial focusing of the beam is canceled by foil and gas scatter, a deposited energy of 0.47 J in the 63 c.c. optical volume, is calculated. This leads to an efficiency of 2.8%. In this calculation an average current density of 8 A/cm^2 over the entire gas cell was assumed for a 40 ns square pulse. Although the coaxial geometry allows the unabsorbed E-beam to be reflected back into the gas, an analysis of the increase in effective beam current due to multiple transit through the laser gas has not been undertaken at this time. However, we believe this contribution can be neglected in the present case because of the rather low cathode voltage and the considerable thickness of the anode foil. The overall electrical efficiency of the original coaxially pumped laser was 0.03%. With further improvements in the pulse rise time and the attendant reduction in foil losses, this number is expected to increase substantially.

This device demonstrates that scalable high pressure E-beam pumped lasers are not merely laboratory curiosities. This is an important step forward because it shows that E-beam excitation, which so far provides the most efficient method of populating the high lying upper electronic levels of visible and UV lasers, is a viable alternative to other more widely accepted excitation methods.

3.2   Quasi-CW Operation of Ar-N_2 Laser.

For the coaxially excited Ar-N_2 laser, described in the previous section, a 50 J Marx was used to drive the cathode. This gave an electron beam pulse width of 40 ns or less. A second Marx bank was constructed using two 0.005 μf at 200 kV Mylar capacitors. These could be charged to their full voltage and switched in series to provide as much as 400 kV at 200 joules. With this Marx bank and a diode impedance of approximately 20Ω the current was over threshold for about 100 ns. Figure 6 shows the timing relation between the current pulse and the output laser pulse. At 20 psia with 5% N_2, the laser is seen to
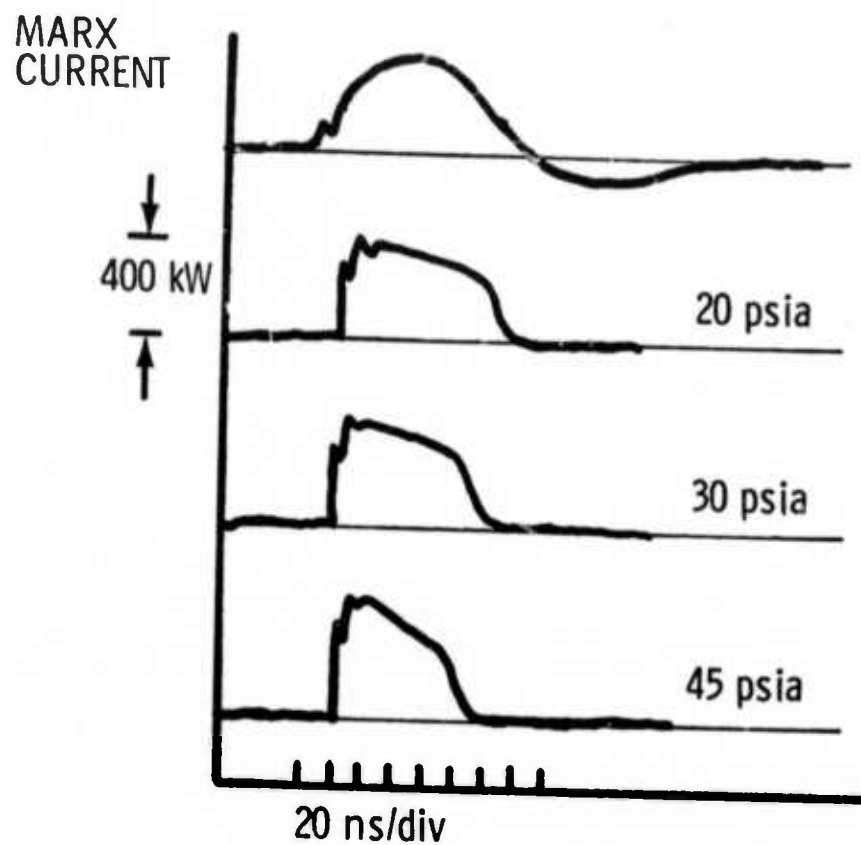
13

Figure 6. Coaxial Ar-N$_2$ laser pulse width compared with
Marx current.   Marx voltage 360 kV, 5% N$_2$ in Ar.

operate in a steady state for 95 ns. This time is well in excess of the longest time constant in the kinetic system, the 40 ns radiative decay time of $N_2(C)$. (Because of collisional quenching, the lifetime is actually shortened by a factor of about 2 at these pressures.) Therefore this experiment clearly established that a quasi-cw operation of the Ar-N_2 system was attained.

The efficiency of the Ar-N_2 laser may be improved if the population of the lower laser level $N_2(B)$ could be utilized for pumping back to the $N_2(C)$ state. Energy pooling reactions offer a possibility to achieve this. However, these reactions usually have a low rate constant, but since the laser is now being operated in a long pulse, the energy pooling reactions may indeed become important. Therefore laser kinetics are presently being examined to see if the energy pooling reaction, $N_2(B) + N_2(A) \rightarrow N_2(C) + N_2(X)$ would be a viable method to recover half of the laser terminal state population and thereby improve the overall laser efficiency. Figure 6 also shows that at higher pressures the laser pulse shortens while the output energy remains approximately the same. We believe this is due to saturation of the lower laser level by a larger extraction rate. A larger extraction rate is desirable to compete against nonradiative quenching from the $N_2(C)$ states. But since the deactivation rate of the lower laser level is limited, a balance between the various rates must be achieved for optimum operation. Under the optimum operating condition for this laser a maximum energy of 130 mJ at an overall efficiency of 0.05% was achieved.

The latest version of the coaxial laser uses a Marx bank with 400 joules at 400 kV giving an even longer current pulse. The pulse is presently limited by the 300 ns closure time of the diode. A laser pulse of 150 ns was obtained using this setup. Figure 7 shows the laser pulse superimposed on the negative going current pulse. The symmetrical location of the laser pulse indicates
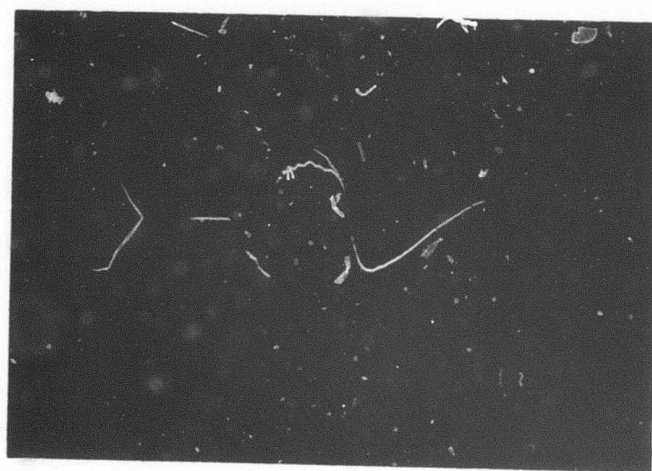
15

Figure 7.   Laser pulse superimposed on the negative
going cathode current pulse. Peak current
~ 10 kA; laser energy ~70 mJ.

the laser operated as long as the current exceeded threshold. Presumably, even longer laser pulses can be obtained with a longer E-beam pulse. Ultimately, gas heating and the foil heating will limit the laser to pulse widths of probably a few microseconds.

3.3   Small Signal Gain Measurements

The small signal gain and the saturation intensity are the two essential parameters necessary for predicting the scaling laws of any laser. The mechanism of operation of the laser may also be best understood by comparing measured small signal gain with the results of kinetic modeling. For these reasons, careful attention was given in developing a technique to measure small signal gain coefficients of the $Ar-N_2$ laser accurately. However, the technique is applicable to any laser of this type.

Because of the difficulty in obtaining a synchronized oscillator pulse of sufficient intensity, a novel technique was employed. Two small (1 cm^2 cross section by 15 cm long) independent gas cells, each fitted with their own optics, were placed side by side and excited by the top and bottom halves of the 2 cm by 10 cm, 1 MeV, 20 ns electron beam. Faraday cups in each cell allowed the current densities to be sampled independently during the 20 ns FWHM E-beam pulse. As shown in Figure 8, the light coupled out of the oscillator was bent 180° by a quartz prism and entered the amplifier after having 7% of the intensity split off by a beam splitter and measured by photodiode O. After passing through the amplifier, the amplified signal was split off to photodiode A. Both photodiodes had S-1 cathodes and had BK-7 diffusers over their faceplates. The pair of diodes were calibrated at 3577Å with radiation from the oscillator, using several shots. The oscillator output was repeatable from shot to shot to approximately ±3%. Careful aperturing and alignment reduced the effects of beam divergence so that more than 90% of the oscillator power passed through the amplifier cavity
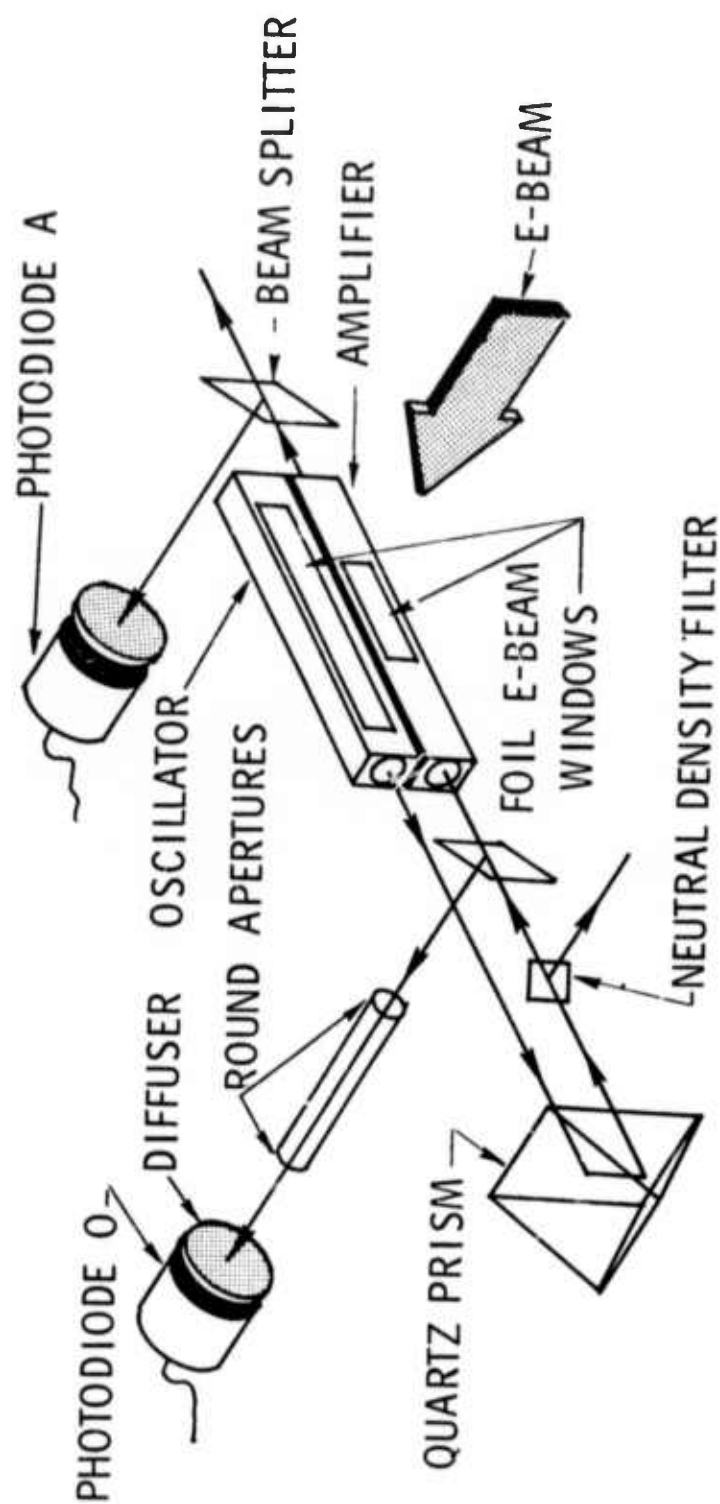
17

Figure 8. Arrangement of the gain measurement experiment.

18

when it was evacuated. The amplifier E-beam was apertured to a gain length of 4.3 cm to prevent saturation and parasitic oscillations and to keep the amplified signal within the dynamic range of photodiode A. The addition of various neutral density filters to the oscillator beam allowed the oscillator power to be varied from zero to a maximum of 125 kW/cm^2. The absolute calibration of the photodiodes was accomplished by integrating the oscillator pulse and comparing this with the total energy measured with a pyroelectric calorimeter.

The signals from the Faraday cup in the amplifier and from both photo-diodes was recorded on a single oscilloscope to preserve the time accuracy. Figure 9 shows a typical oscilloscope trace and the cable connections. Figures 10 and 11 show typical plots of the experimental data. For the data in Figure 10, the pressure was monitored at 4.8 atm but the mixture was varied from 5% to 2%. The reduction in gain and the saturation intensity followed the reduction in N_2 concentration. The results at the near optimum concentration of 5%, shown in Figure 11, indicate only a slight change in amplifier performance with a change in pressure of 3 atm to 4.8 atm. The peak current of the beam, measured with the Faraday cup in the amplifier, was 2.9 kA/cm^2 for all the experiments described herein.

The single pass gain in a high gain amplifier can be analyzed as follws: The gain coefficient as a function of distance is given by

$$\alpha(x) = \frac{1}{I(x)} \frac{dI(x)}{dx} \tag{1}$$

where $I(x)$ is the radiation intensity at a given location x along the axis of the amplifier. As the intensity increases towards saturation, the saturated gain
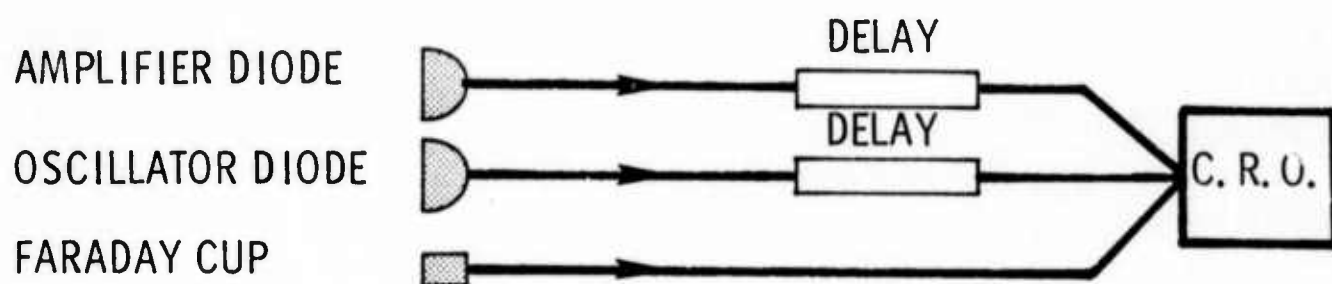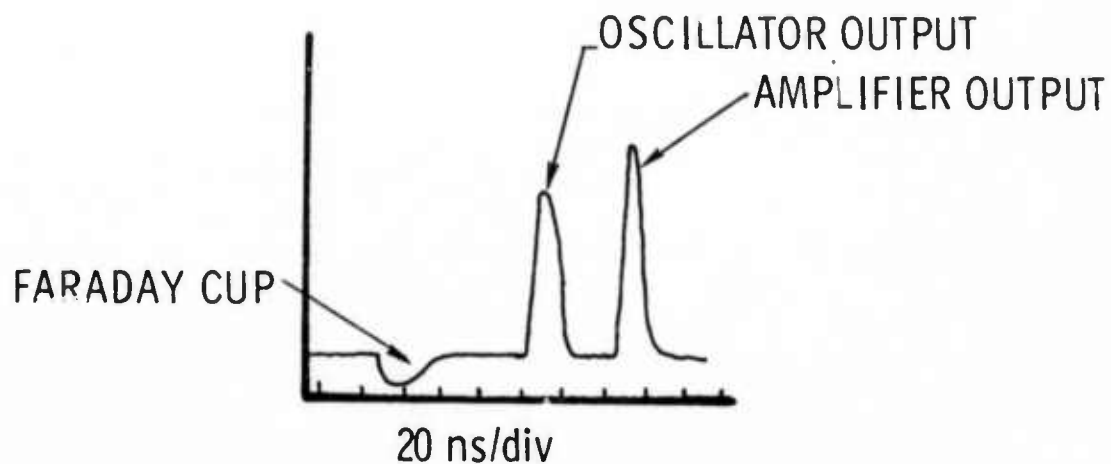
Figure 9. Oscilloscope trace and the corresponding cable
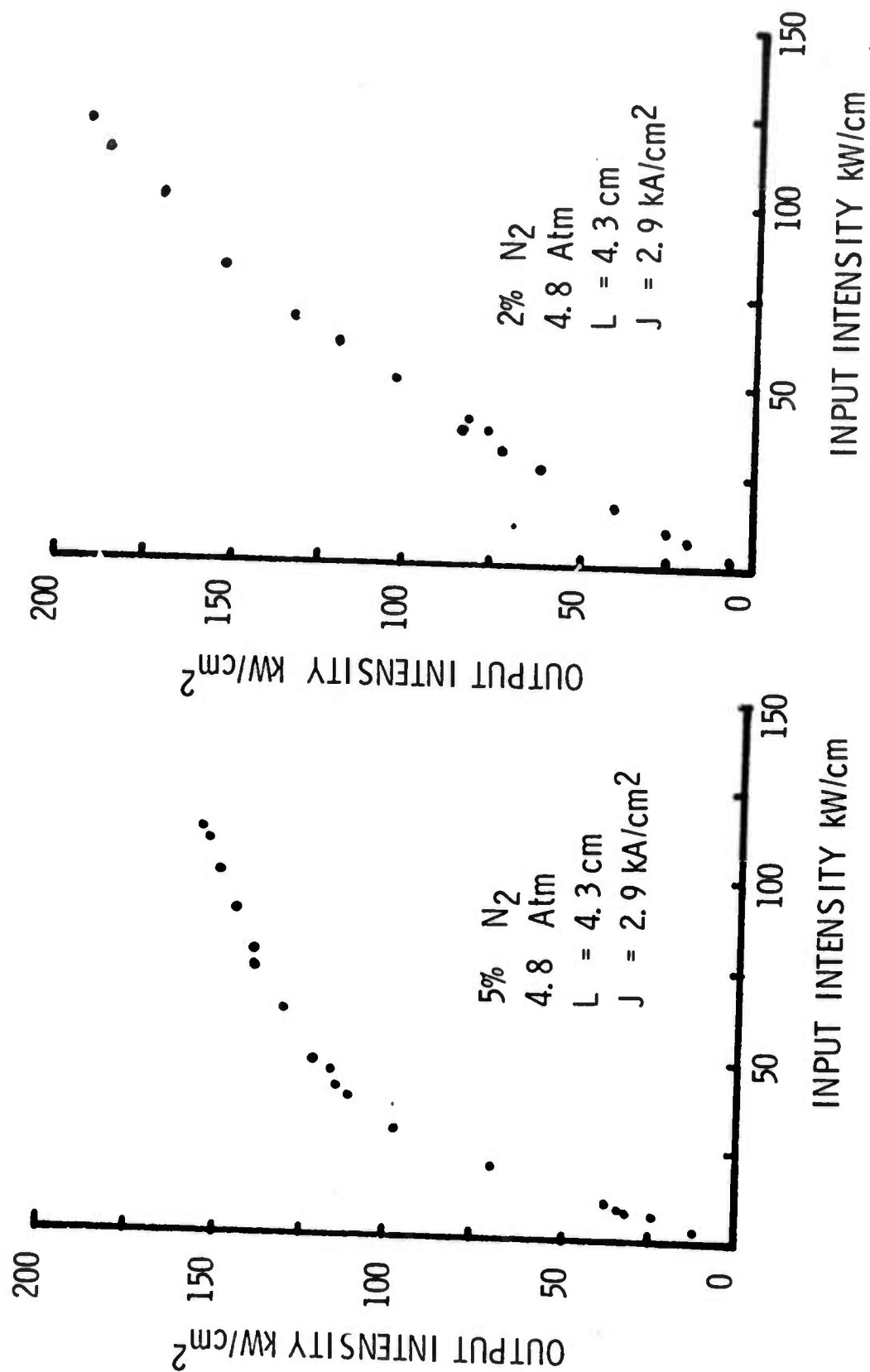connections for the gain measurement experiment.

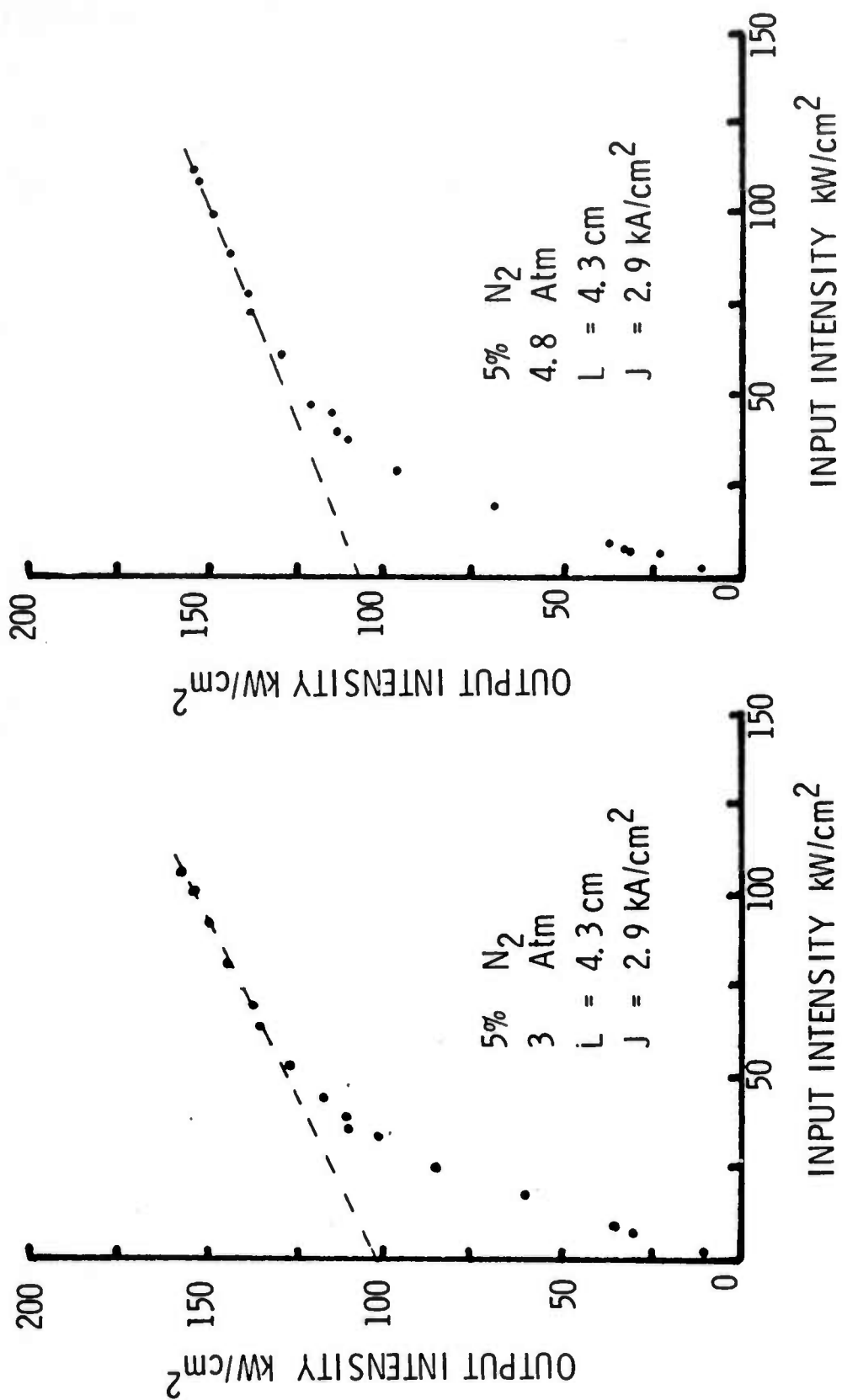Figure 10. Ar-N$_2$ amplifier characteristics at constant pressure.

21

Figure 11. Ar-N_2 amplifier characteristics at constant mixture.

coefficient can be given as a function of the small signal gain coefficient, α_0, and the saturation intensity I_s by the expression

$$\alpha(x) = \frac{\alpha_0}{1 + I(x)/I_s} \tag{2}$$

Combining (1) and (2) and integrating over the length of the gain medium, L, yields

$$\ln\left[\frac{I_{out}}{I_{in}}\right] + \frac{I_{out} - I_{in}}{I_s} = \alpha_0 L \tag{3}$$

Here I_{out} and I_{in} are the amplifier output and input intensities. The length, L, must be chosen small enough to prevent saturation of the medium at small I_{in} values. In the limit of small I_{in} and therefore small I_{out} compared to I_s, Equation (3) reduced to

$$I_{out} = I_{in} e^{\alpha_0 L} \tag{4}$$

As I_{in} becomes large compared to I_s, Equation (3) becomes

$$I_{out} = I_{in} + \alpha_0 L I_s. \tag{5}$$

Figure 12 shows schematically these two limits. At small I_{in} the slope gives the small signal gain. At large I_{in} the slope must approach unity since the output equals the input plus the maximum extractable energy from the medium, $\alpha_0 L I_s$. The intercept of the slope on I_{out} gives $\alpha_0 L I_s$.

The small signal gain α_0, derived from the intensity measurements, is shown in Figure 13 at two different pressures and various mixture ratios. The maximum gain of 37% per cm was obtained for a 10% mixture at 4.8 atm total pressures. The gain peaked at 30% per cm for a 5% mixture and total
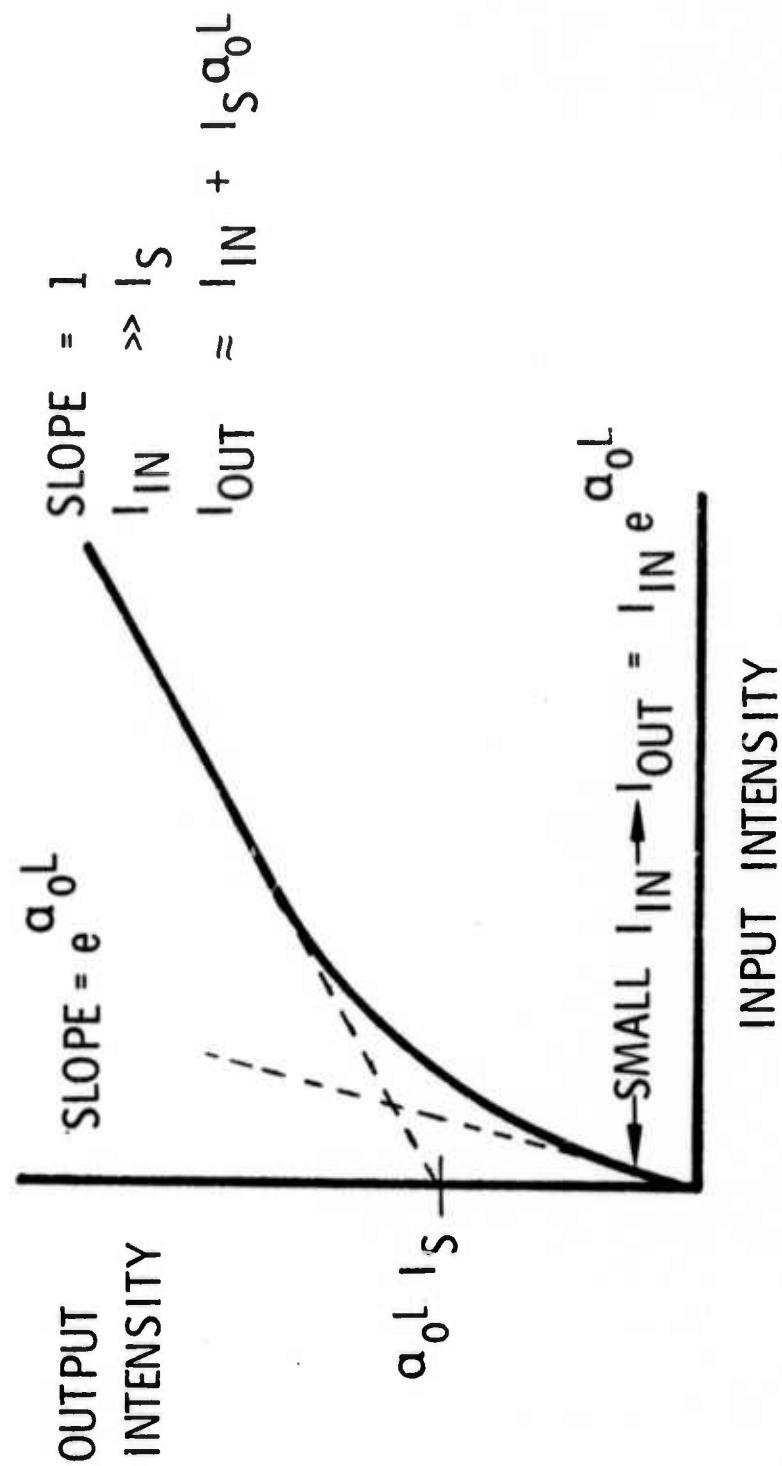
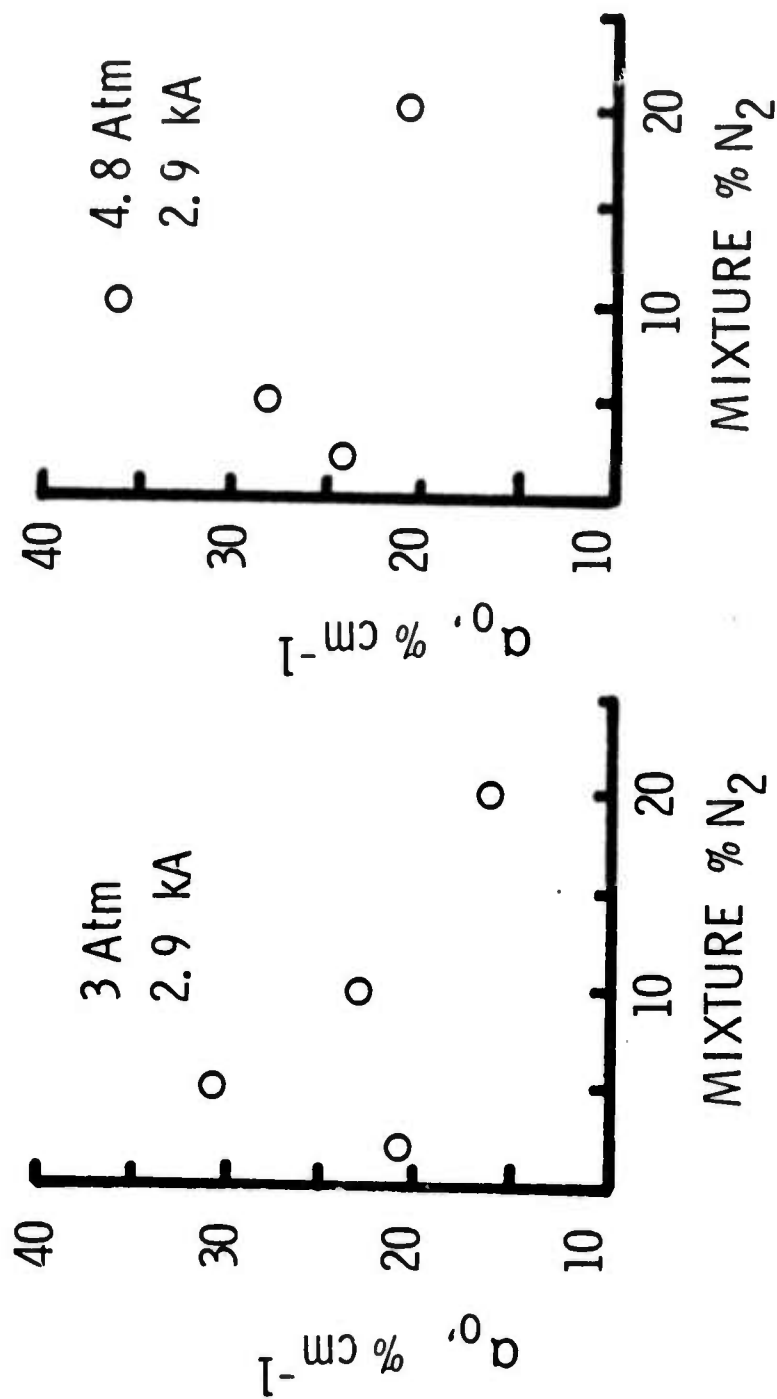Figure 12. Laser amplifier characteristic curve.

Figure 13. Ar-N_2 small signal laser gain vs % N_2.

pressure of 3 atm. These optimum gain values correlate well with the optimum pressures and mixtures obtained by adjusting the Ar-N₂ laser for maximum output energy. Also, work is now under way to correlate these data to the results of kinetic modeling. The saturation intensity I_s is calculated to be 100 kW/cm² from these measurements. This value agrees excellently with that derived from the plot of laser intensity vs current density.

3.4 Kinetic Modeling of Ar-N₂ Laser.

The predominant mechanism by which energy from a high energy E-beam is absorbed by Ar is by ion-electron pair production. The relativistic (high energy) electron produces[2] 3.5 Ar⁺ and 1 Ar* by losing 91 eV. Any energy in excess of the ionization and atomic excitation energy appears as the energy of the secondary electrons. But the secondary electrons may be assumed to cool rapidly due to a high collision rate in the high pressure gas; therefore pumping of Ar or N₂ by secondary electrons is not expected to make a significant contribution. The energy pumping by ion-electron pair production was introduced into the computer program in the form of a cross section using the following equation:

$$\frac{dn(Ar^+)}{dt} = \frac{J}{e} \, n(Ar) \, \sigma(+)$$

where $n(Ar^+)$ is the number density of Ar ions, J is the current density, e the electronic charge, n(Ar) the number density of Ar atoms and $\sigma(+)$ is the cross section for producing Ar^+. A similar cross section $\sigma(*)$ was derived for the production of Ar* by high energy electrons.

Since 3.5 Ar⁺ and 1.0 Ar* are produced for each 91 eV loss of E-beam energy,

$$\sigma(+) \, n(Ar) = 3.5 \, \frac{dE/dx}{91}$$

$$\sigma(*) \, n(Ar) = \frac{dE/dx}{91}$$

26

Taking $dE/dx = 2.5$ keV/cm at 1 atm of Ar (300°K),[1]

$$\sigma (+) \quad = \quad 3.85 \times 10^{-18} \; cm^2$$

$$\sigma (*) \quad = \quad 1.1 \times 10^{-18} \; cm^2$$

The rest of the analysis is rather straightforward even though the Ar excitation followed by energy transfer to N_2 and relaxation processes in N_2 involves a large number of reactions. The task is, however, made difficult due to lack of accurate knowledge of the rate constants of some of the key reactions. In the present model, all the possible processes judged to be pertinent are included and are shown in Table I. The best available rate constants of these processes, taken from published data, are shown in Table II. The unknown rates or those which seem to be negligible are taken as 0 for the present.

The set of differential equations constructed to represent the processes shown in Table I together with their rate constants given in Table II were solved by using a CDC 6600 computer. A Runge-Kutta integration technique was used which resulted in the smallest integration time. In addition to the normal tabulation of the results, a plot routine was used to display a population density vs time plot. Figures 14, 15, and 16 show the population densities of the various species due to excitation of 4 atm Ar + 5% N_2 by a 2.5 kA, 20ns E-beam. These plots are typical of a large number of plots representing various pressures, mixtures, and current densities. In all of these cases, the population density of N_2(B), the lower laser level was higher. This is consistent with the experimental result that the laser does not operate on the N_2(C) $v' = 0 \rightarrow N_2$(B) $v'' = 0$. But N_2(B) $v'' = 1$, situated 1734 cm^{-1} above the $v'' = 0$, has a population 2.7×10^{-4} that of $v'' = 0$. For the examples given here the peak population of N_2(C) is 7.5×10^{15}/c.c. The corresponding population of the N_2(B)$v'' = 0$ and $v'' = 1$ levels are 5×10^{16}/c.c. and 1.4×10^{13}/c.c. respectively, assuming vibrational equilibrium in the N_2(B)
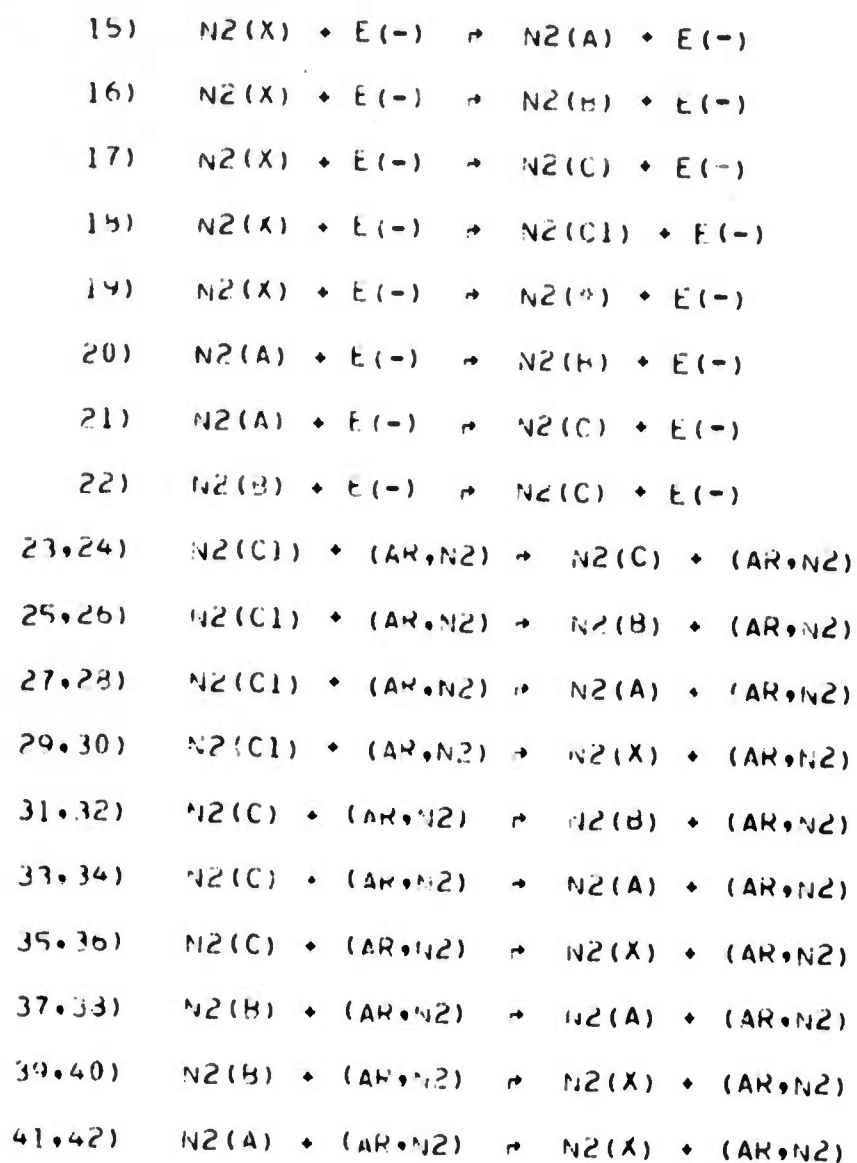
Table I.   Reactions Assumed in the Present Kinetic Model

REACTIONS INVOLVING EXCITATION AND KINETICS OF THE EXCITED
AR SPECIES --

0)   AR(0) + HE(-) → AR(+) + HE(-) + E(-)
     CURRENT = THEAM, CROSS SECTION = SIGMA

1)   AR(0) + E(-) → AR(+) + E(-)

2)   AR(+) + AR(0) + AR → AR2(+) + AR

3)   AR(+) + AR(0) + N2 → AR2(+) + N2

4)   AR2(+) + E(-) → AR(*) + AR(0)

5)   AR(*) + AR(0) + AR → AR2(*) + AR

6)   AR(*) + AR(0) + N2 → AR2(*) + N2

7)   AR2(*) + E(-) → AR(0) + AR(0) + E(-)

8)   AR(*) + AR(*) → AR(+) + AR(0) + E(-)

9)   AR2(*) + AR2(*) → AR2(+) + 2AR(0) + E(-)

10) AR2(*) → AR(0) + AR(0) + HNU

11) AR(0) + E(-) → AR(*) + E(-)

12) AR(*) + AR → AR(0) + AR

13) AR(*) + N2 → AR(0) + N2

14) AR(*) → AR(0) + HNU

28

Table I. Reactions Assumed in the Present Kinetic Model (continued)

REACTIONS INVOLVING EXCITATION AND KINETICS OF THE EXCITED
N2 SPECIES --

$$15) \quad N2(X) + E(-) \rightarrow N2(A) + E(-)$$

$$16) \quad N2(X) + E(-) \rightarrow N2(B) + E(-)$$

$$17) \quad N2(X) + E(-) \rightarrow N2(C) + E(-)$$

$$18) \quad N2(X) + E(-) \rightarrow N2(C1) + E(-)$$

$$19) \quad N2(X) + E(-) \rightarrow N2(*) + E(-)$$

$$20) \quad N2(A) + E(-) \rightarrow N2(B) + E(-)$$

$$21) \quad N2(A) + E(-) \rightarrow N2(C) + E(-)$$

$$22) \quad N2(B) + E(-) \rightarrow N2(C) + E(-)$$

$$23,24) \quad N2(C1) + (AR,N2) \rightarrow N2(C) + (AR,N2)$$

$$25,26) \quad N2(C1) + (AR,N2) \rightarrow N2(B) + (AR,N2)$$

$$27,28) \quad N2(C1) + (AR,N2) \rightarrow N2(A) + (AR,N2)$$

$$29,30) \quad N2(C1) + (AR,N2) \rightarrow N2(X) + (AR,N2)$$

$$31,32) \quad N2(C) + (AR,N2) \rightarrow N2(B) + (AR,N2)$$

$$33,34) \quad N2(C) + (AR,N2) \rightarrow N2(A) + (AR,N2)$$

$$35,36) \quad N2(C) + (AR,N2) \rightarrow N2(X) + (AR,N2)$$

$$37,38) \quad N2(B) + (AR,N2) \rightarrow N2(A) + (AR,N2)$$

$$39,40) \quad N2(B) + (AR,N2) \rightarrow N2(X) + (AR,N2)$$

$$41,42) \quad N2(A) + (AR,N2) \rightarrow N2(X) + (AR,N2)$$

NEAR RESONANT (CROSS RELAXATION) PROCESSES AMONG THE
EXCITED N2 STATES --

$$43) \quad N2(A) + N2(A) \rightarrow N2(C1) + N2(X)$$

$$44) \quad N2(A) + N2(A) \rightarrow N2(C) + N2(X)$$

$$45) \quad N2(B) + N2(B) \rightarrow N2(C) + N2(X)$$

$$46) \quad N2(A) + N2(B) \rightarrow N2(C) + N2(X)$$

$$47) \quad N2(A) + N2(C) \rightarrow N2(B) + N2(B)$$

$$48) \quad N2(A) + N2(A) \rightarrow N2(B) + N2(X)$$
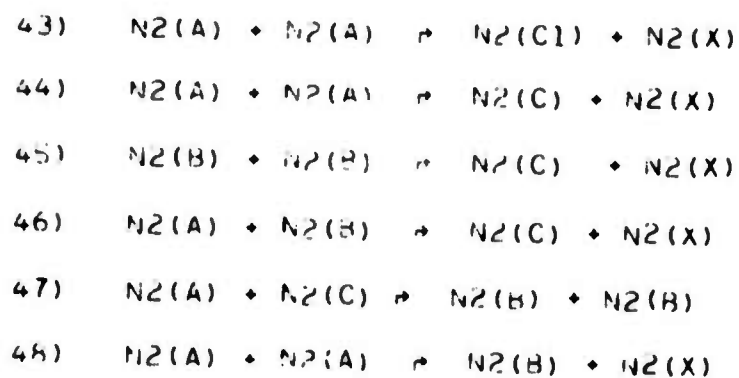
Table I. Reactions Assumed in the Present Kinetic Model (continued)

SPONTANEOUS RADIATIVE DECAY PROCESSES FOR THE EXCITED N2 STATES--

49) $N2(C) \rightarrow N2(B) + HNU$

50) $N2(C) \rightarrow N2(A) + HNU$

51) $N2(C) \rightarrow N2(X) + HNU$

52) $N2(B) \rightarrow N2(A) + HNU$

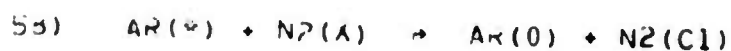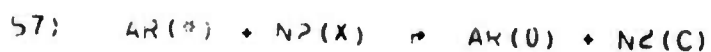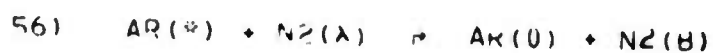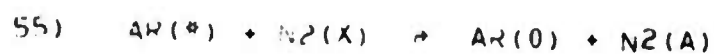53) $N2(B) \rightarrow N2(X) + HNU$

54) $N2(A) \rightarrow N2(X) + HNU$

RESONANT ENERGY EXCHANGE (CROSS-RELAXATION) REACTIONS --

55) $AR(*) + N2(X) \rightarrow AR(0) + N2(A)$

56) $AR(*) + N2(X) \rightarrow AR(0) + N2(B)$

57) $AR(*) + N2(X) \rightarrow AR(0) + N2(C)$

58) $AR(*) + N2(X) \rightarrow AR(0) + N2(C1)$

59) $AR(*) + N2(X) \rightarrow AR(0) + N2(*)$

60) $AR2(*) + N2(X) \rightarrow 2AR(0) + N2(A)$

61) $AR2(*) + N2(X) \rightarrow 2AR(0) + N2(B)$

62) $AR2(*) + N2(X) \rightarrow 2AR(0) + N2(C)$

63) $AR2(*) + N2(X) \rightarrow 2AR(0) + N2(C1)$

64) $AR2(*) + N2(X) \rightarrow 2AR(0) + N2(*)$
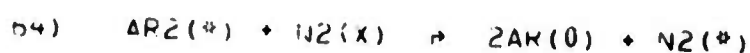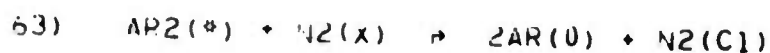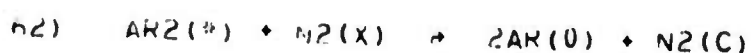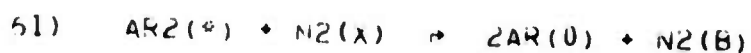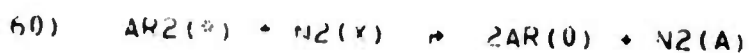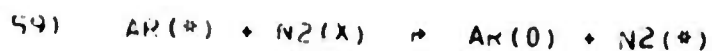
MISCELLANEOUS REACTIONS WITH OTHER SPECIES --

65) $N2(A) + NO(X) \rightarrow N2(X) + NO(A)$

66,67) $NO(A) + (AR,N2) \rightarrow NO(X) + (AR,N2)$

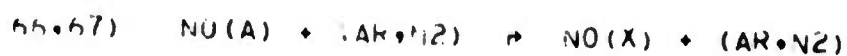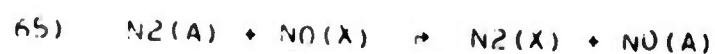68) $NO(A) \rightarrow NO(X) + HNU$

30

Table II. Rate coefficient in cm^6/sec or cm^3/sec for the reactions given in Table I. KF(I) and KF(R) denote the rate of forward and backward reactions, respectively.

| Reaction Number	KF(I)	KR(I)	Reaction Number	KF(I)	KR(I)
1	0.	0.	41	0.	0.
2	2.5000E-31	0.	42	0.	0.
3	0.	0.	43	1.0000E-11	0.
4	1.0000E-06	0.	44	1.0000E-11	0.
5	1.0000E-32	0.	45	1.0000E-13	0.
6	0.	0.	46	0.	0.
7	1.0000E-09	0.	47	0.	0.
8	5.0000E-10	0.	48	8.0000E-11	0.
9	5.0000E-10	0.	49	2.2000E+07	0.
10	2.4000E-07	0.	50	0.	0.
11	0.	0.	51	0.	0.
12	0.	0.	52	1.2000E+05	0.
13	0.	0.	53	0.	0.
14	0.	0.	54	0.	0.
15	0.	0.	55	0.	0.
16	0.	0.	56	1.7000E-11	0.
17	0.	0.	57	3.0000E-12	0.
18	0.	0.	58	1.0000E-11	0.
19	0.	0.	59	0.	0.
20	0.	0.	60	0.	0.
21	0.	0.	61	1.0000E-11	0.
22	0.	0.	62	0.	0.
23	3.0000E-12	0.	63	0.	0.
24	0.	0.	64	0.	0.
25	0.	0.	65	8.0000E-11	0.
26	0.	0.	66	0.	0.
27	0.	0.	67	0.	0.
28	0.	0.	68	0.	0.
29	0.	0.			
30	0.	0.			
31	8.0000E-13	0.			
32	1.1000E-11	0.			
33	0.	0.			
34	0.	0.			
35	0.	0.			
36	0.	0.			
37	1.0000E-14	0.			
38	2.6000E-12	0.			
39	0.	0.			
40	0.	0.			
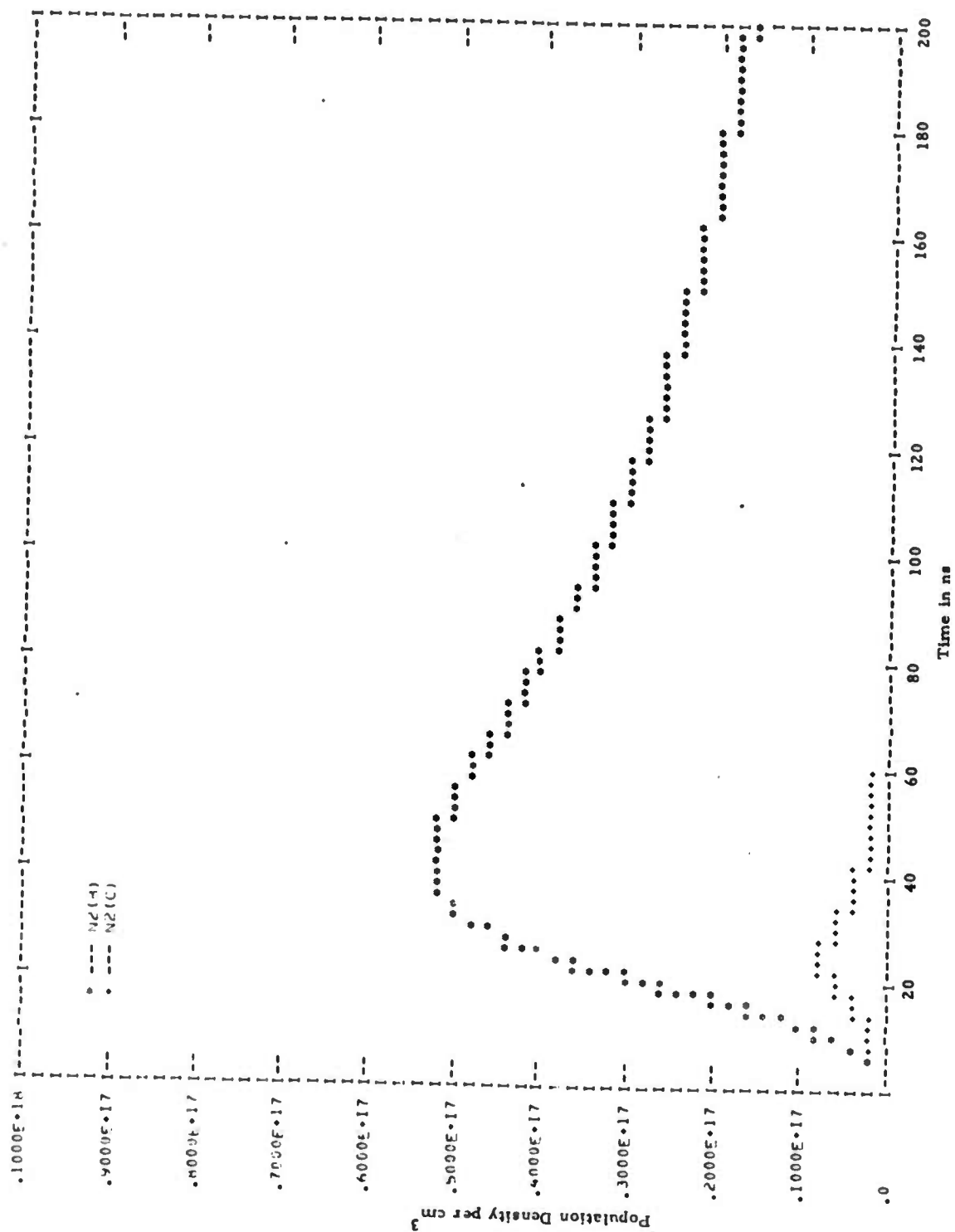
Figure 14. Population densities of $N_2(B)$ and $N_2(C)$ vs time due to excitation of 3 atm Ar + 5% N_2 by a 2.5 kA, 20 ns beam.
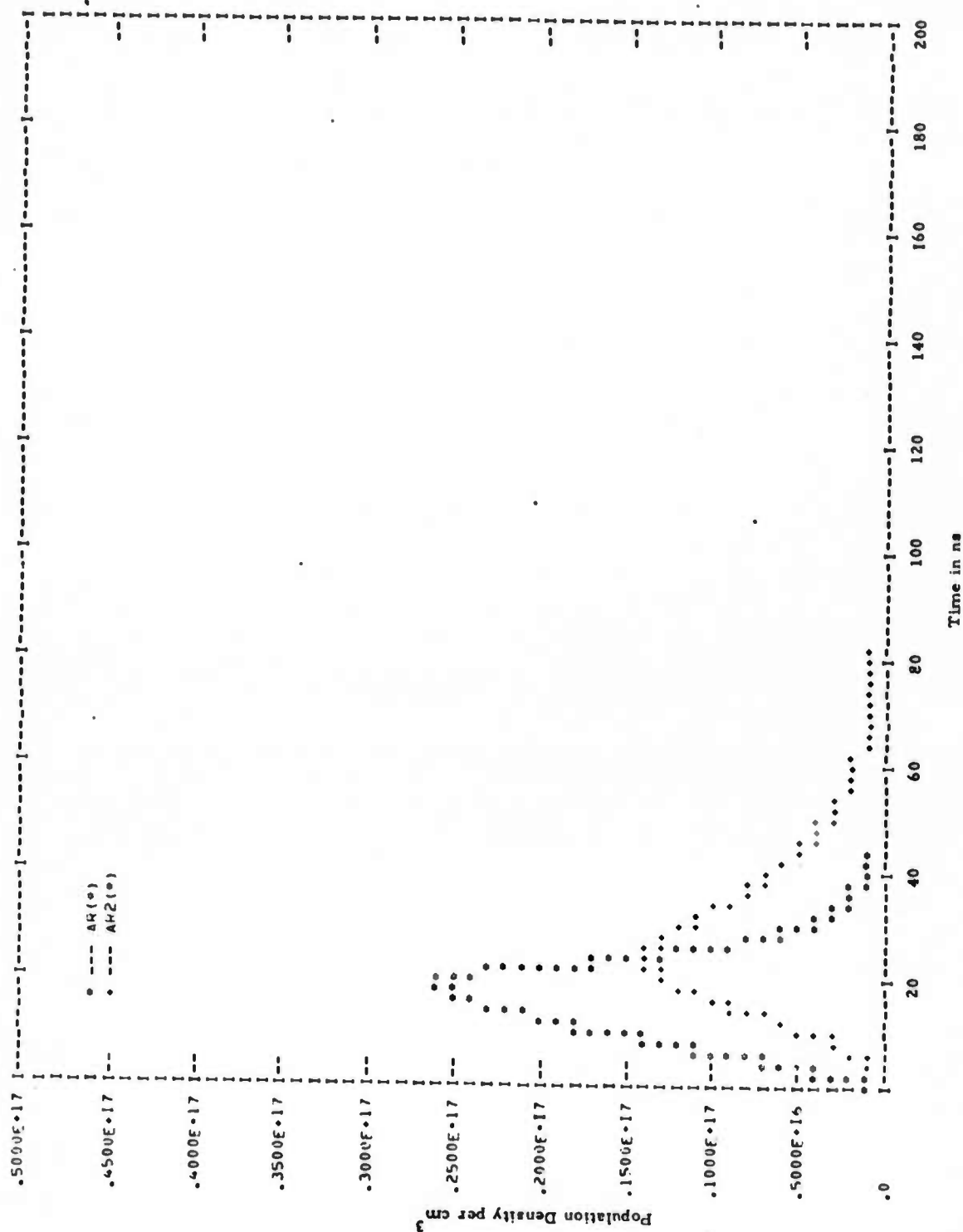
32

Figure 15. Population density of Ar^* and Ar_2^* vs time due to excitation of 3 atm Ar + 5% N_2 by a 2.5 kA, 20 ns beam.
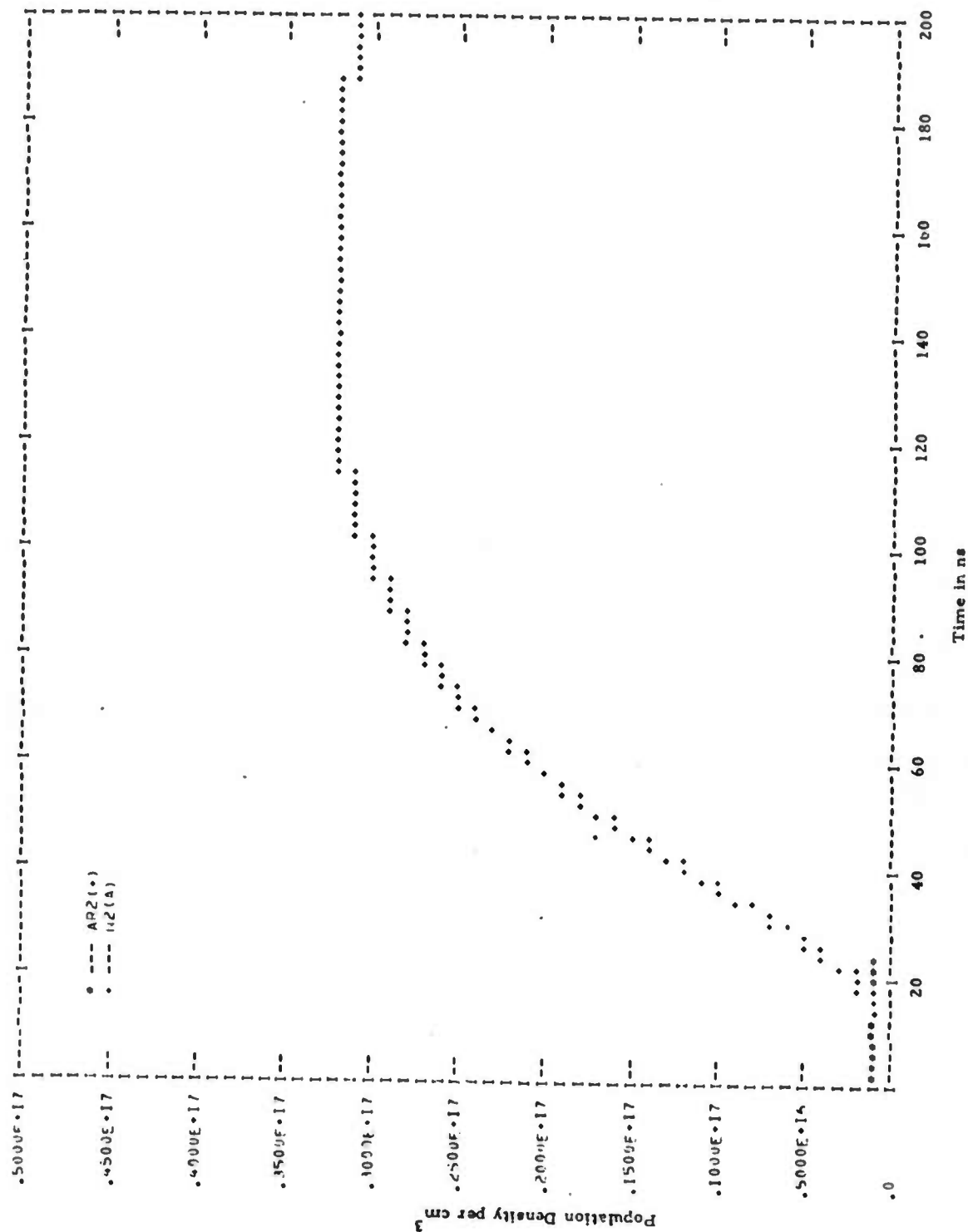
Figure 16. Population density of $N_2(A)$ vs time due to excitation of 3 atm Ar + 5% N_2 by a 2.5 kA, 20 ns beam.

34

state, Therefore, the inversion between $N_2(C)$ $v' = 0$ and $N_2(B)$ $v'' = 1$ is obvious. Of course, an inversion may also exist between $N_2(C)$ $v' = 0$ and still higher vibrational levels of $N_2(B)$.

The best means to test the validity of modeling is by comparing the above population with those derived from the measurement of small signal gain, presented in Section 3.3. Knowing the population of the $N_2(C)$ and $N_2(B)$ states, the theoretical value of the gain can be derived in the following way.

The small signal gain coefficient α_0 for a transition from state b to state a is given by

$$\alpha_0 = \frac{A_{ba} \; \lambda_{ba}^2}{8 \pi c \; \Delta \nu} \; N_b \left(1 - \frac{g_b \; N_a}{g_a \; N_b} \right) \tag{6}$$

where A_{ba} is the spontaneous transition probability, λ_{ba} is the wavelength of the transition, $\Delta \nu$ is the linewidth, $N_b(N_a)$ is the upper (lower) state population, and $g_b(g_a)$ is the upper (lower) state degeneracy.

To calculate the gain for N_2 $C\,^3\Pi_u \rightarrow B\,^3\Pi_g$ (0, 1) transitions, we assume a pressure broadened linewidth of 1 cm^{-1} and that laser action occurs from a single rotational level having the largest population. Even with 1 cm^{-1} pressure broadening, the three Π sub-bands should be distinct. Figure 19 is a Fortrat diagram constructed for the N_2 C-B (0, 0) system which should be quite similar to (0, 1). It is interesting to note that the band head is close to the level of maximum population at 300 K and that sub-bands are separated by more than 3 cm^{-1}.

For a given rotational level, the $^3\Pi$ state therefore has 3 sub-bands, $^3\Pi_2$, $^3\Pi_1$, and $^3\Pi_0$, each having two Λ-doubling components. Parks, et al.[3] have indicated that one Λ-component of each Π sub-state has much larger gain than the other. In a state with total population N, the population as a
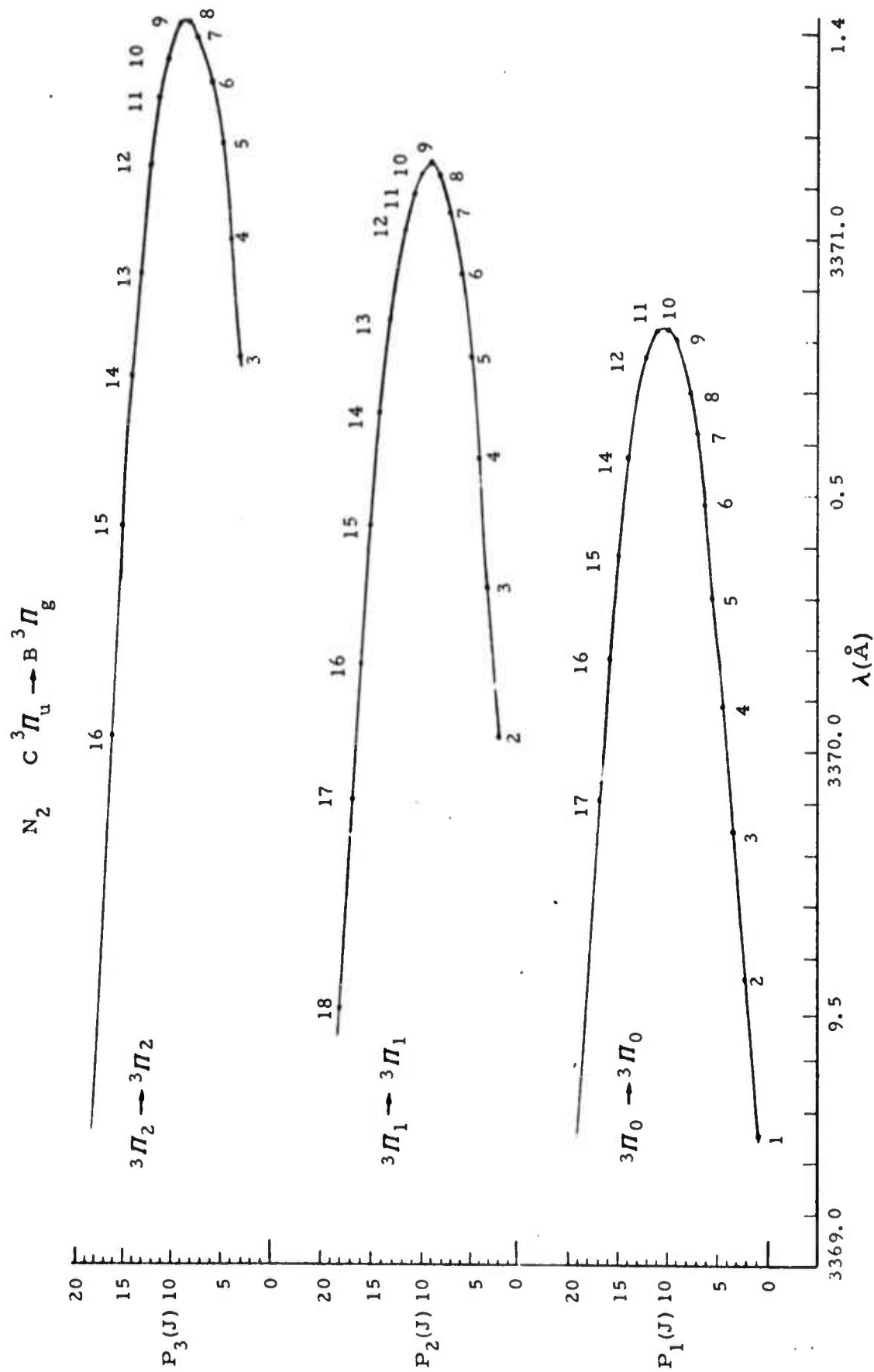
Figure 17. Fortrat diagram for N_2 second positive transitions.

function of J is:[4]

$$N(J) = \frac{N \, hc \, B}{kT} (2J + 1) \exp - \left\{ BJ(J+1)\frac{hc}{kT} \right\}$$ (7)

where B is the rotational constant and T is the rotational temperature. This distribution peaks at:[4]

$$J_{max} = \sqrt{\frac{kT}{2B \, hc}} - \frac{1}{2}$$ (8)

In the case of N_2 C $^2\Pi$, B = 1.83 cm^{-1} and T is assumed to be 300 K, so that Equation (8) yields J_{max} = 7 and Equation (7) gives N(t) = 0.080 N, which must be reduced by a factor of 6 for a given Λ-component of a specific Π sub-band. Now for the C $^3\Pi$ state, our kinetics model shows that N = 7.5 x 10^{15} cm^{-3} so that the population of the upper lasing state is

$$N_b = \left(\frac{0.080}{6} \right) (7.5 \times 10^{15} \, cm^{-3})$$

$$= 1.00 \times 10^{14} \, cm^{-3}$$

For the present, assume that $N_b \gg N_a$ so that Equation (6) with $\Delta \nu = 1$ reduces to:

$$\alpha = \frac{A_{ba} \lambda_{ba}^2}{8 \pi c} N_b$$ (9)

Using A = 7.33 x 10^6 sec from Schemansky and Broadfoot[5] and λ = 357.6 nm in (9), we obtain

$$\alpha = 1.24 \, cm^{-1}$$ (10)

which is five times the measured value.

The reason for the discrepancy between the measured and calculated values of the small signal gain coefficient is not yet clear. One souce of error might be the measured value of the current density. In these experiments the Faraday probe was quite close to the gas cell foil since the laser amplifier cross sectional dimension was small. There is a possibility that the Faraday cup was monitoring the current in a hot spot of the E-beam. In an actual laser experiment using a much larger gas volume, such hot spots will be diffused by the gas scattering. In these oscillator-amplifier experiments, it was not accurately known to what extent the hot spot was responsible for pumping the total 4.8 cm long amplifier. Since a total cathode current is measured for a 2 x 10 cm E-beam, the average current density would normally be ~ 1 kA/cm^2. If this was the case, the calculated gain value will be reduced by a factor of 3 and would be closer to the measured value. Further experiments are contemplated to clarify this situation.

There are several other quantities whose values are not known accurately. These may also affect the gain calculations. A branching ratio of transfer from Ar to N$_2^*$, vibrational specificity of transfer, extent of vibrational equilibration, the rise in gas temperature and the particular spectral lines in the laser spectrum are among these unknowns. A more accurate gain prediction can be made only after more data is available.

3.5   Overvoltaged Discharge Studies

Experiments to date using the coaxial geometry show that efficient operation of the Ar-N$_2$ laser occurs at pressures as low as 1 atm. This indicates that it may be possible to develop a scalable discharge pumped rare gas transfer laser at these low pressures. Even if the laser efficiency were to be lower than the E-beam pumped Ar-N$_2$ laser, the overall device efficiency may be higher at least for some operating conditions. Mixtures of rare gases with a

small percentage of a diatomic molecule such as N_2 can be excited by a discharge, although a part of the input energy may appear as vibrational excitation of the diatomic species. At pressures near 1 atm and with a fast, overvoltaged discharge, it should be possible to get a large enough ratio of E/N to create a population of high temperature electrons that will excite the rare gas metastable and therefore allow for selective population of the $N_2(C)$ states.

A 20 cm long plastic discharge plenum was constructed and fitted with one inch diameter optics. The stabilizing electron beam was supplied by a razor blade cathode driven by a 500 kV, 50 joule Marx bank. The repetition rate of this device was 1 Hz. This plenum was limited to pressures less than 5 atm because of sealing problems. At the time these experiments were undertaken, only aluminum coated mirrors were available.

Various mixtures of Ar-N_2 at pressures reaching 3 atm were tried but laser oscillations were not observed. Even though the sustainer discharge was able to produce five times the fluorescence from $N_2(C)$ than the stabilizing E-beam ($\sim 3A/cm^2$ for 20 ns), laser threshold could not be reached with the available mirrors. Figure 18 shows a typical photodiode measurement of the UV fluorescence from the discharge. The peak power of the discharge fluorescence was 20 watts over a 2 cm diameter aperture. Further work was deferred in favor of the coaxial laser development but these experiments show that the upper laser levels of nitrogen can indeed be populated by energy transfer from discharge pumped argon. Pure nitrogen in the same discharge at the same pressure yields almost no emission compared to the case of Ar-N_2 mixtures.

FLUORESCENCE FROM
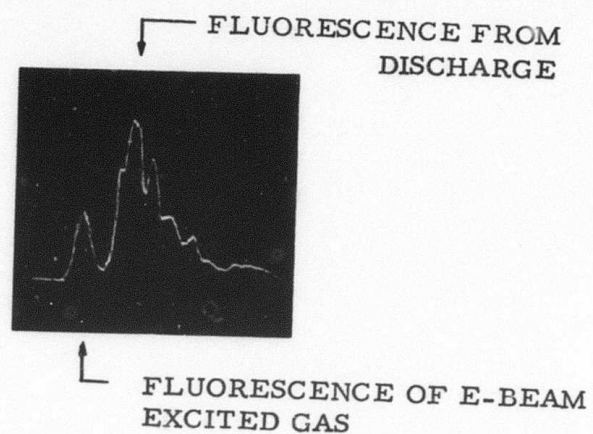DISCHARGE

FLUORESCENCE OF E-BEAM
EXCITED GAS

Figure 18.   UV fluorescence of an E-beam initiated
discharge at 2 atm with 5% N_2 in argon.
The E-beam portion of this trace (the
first bell shaped peak) is 20 ns FWHM.

3.6   High Energy Xenon Laser Development.

A xenon laser development program was initiated under the sponsorship of the Defense Nuclear Agency (DNA).   The scope of the work included the installation and checkout of an E-beam gun, the design and construction of a xenon laser and optimization of the laser for the highest output energy.   The E-gun supplied by DNA was a Physics International model 535, capable of delivering 100 kA at 3 MeV in a 60 ns pulse. However, the DNA sponsorship only supported some initial laser experiments.   Further work was done with ARPA/ONR support.

These efforts resulted in a maximum laser output of 10 joules in 25 ns FWHM using all-dielectric optics.   Attempts to increase the laser output further were limited by the destruction of the optical components because of the intense laser beam.   Even at lower powers, the mirrors were degraded after a few shots.   At this time optical damage indeed seems to be the mechanism that limits the maximum energy which can be extracted from a VUV xenon laser. The details of these studies are described below.

The experimental arrangement for these studies is shown in Figure 19.   The laser gas was excited in the direction transverse to the optical axis.   To insure that impurity quenching would be negligible, the entire gas cell was hard sealed and pumped with an oil free ultrahigh vacuum pump system. Furthermore, the xenon was distilled in an all stainless steel gas recovery system.   This system also allowed the xenon to be reclaimed from the laser.

With stable dielectric optics it was easy to reach threshold at pressures as low as 80 psia.   Even with the electron beam intensity reduced by a factor of 3, optical damage was observed after several shots.   One shot at full pressure (150 psia) and maximum beam energy would destroy the coatings and, if
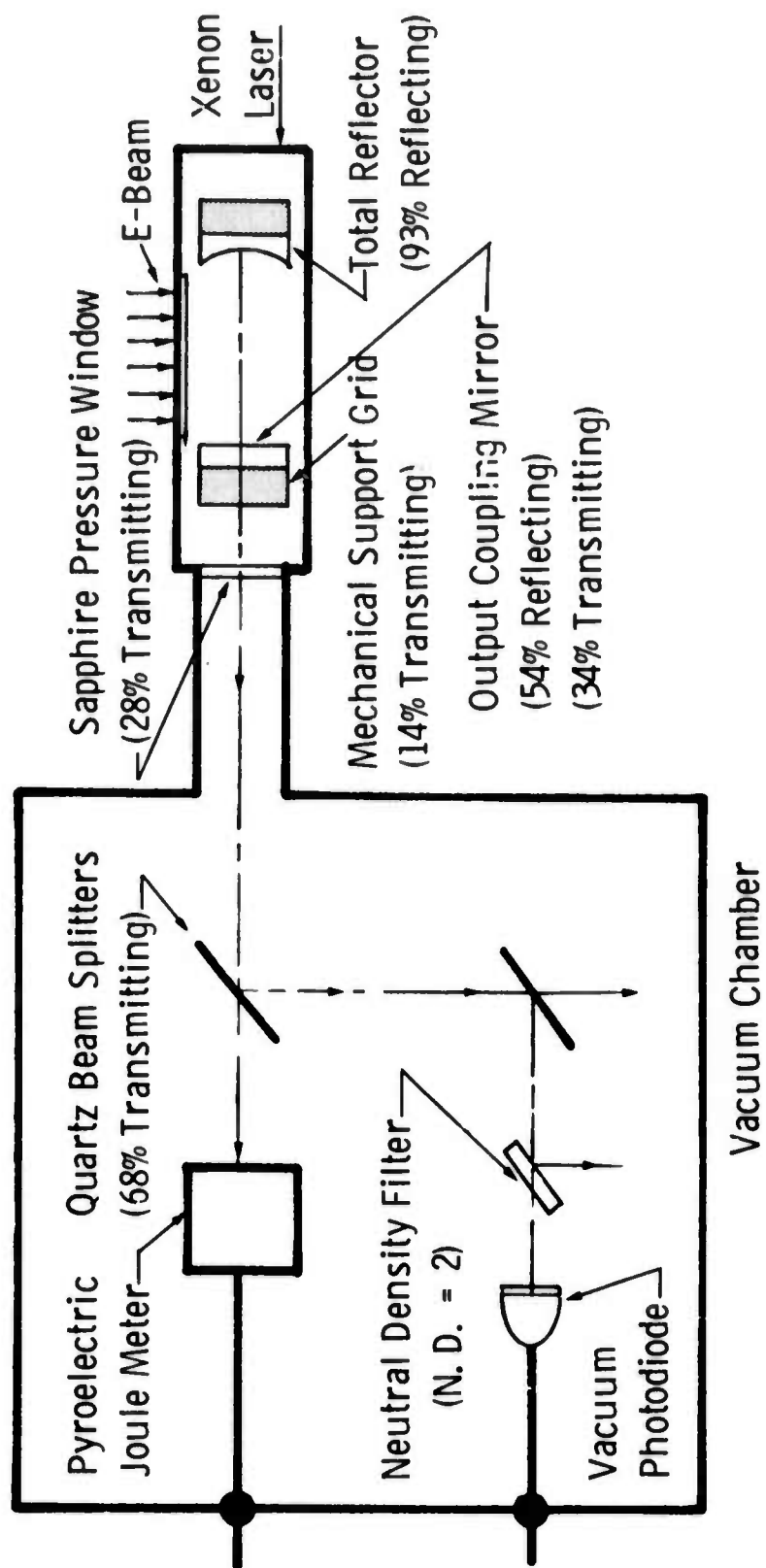
41

Figure 19. Schematic diagram of the optical diagnostics for the vacuum UV xenon laser.

not adequately supported, destroy the substrate also. However, under these conditions, a maximum of 10.6 joules was extracted from the laser. We believe that this energy is extracted before the mirrors are destroyed. The laser efficiency, based on energy absorption, was calculated to be ~6%.

The transmission of the pressure window and the optical components was determined by a vendor with a vacuum UV spectrophotometer. The transmission of the mechanical support grid was deduced by calculation. In addition to the factor of 10 reduction in intensity afforded by the first beam splitter, a further factor of 1000 was supplied by another beam splitter and a 1% transmitting neutral density filter so that the photodiode would not saturate. The overall transmission from the laser cavity to the photodiode is of the order of 10^{-7}.

Figure 20(a) shows the photodiode output for this shot. The laser rapidly crosses threshold as the current rises (see Figure 20(b)), exhibits a small gain switching spike, and rapidly decays after 25 ns. With this pulsewidth and a total energy of 10 J, the peak power is 400 MW. Inside the laser cavity the power is a factor of 2 higher because only 50% of the laser circulating power is coupled out. These high powers combined with the inherent absorption of dielectric materials presently available for coatings explain why it is impossible to fabricate present state-of-the-art optical components which will not damage.

In conclusion, a high energy vacuum UV xenon laser was constructed and tested which produced a 25 ns, 400 MW, 10 joule pulse. This represents a step forward in the study of this part of the spectrum. To our knowledge this is the highest energy obtained from a xenon laser. Due to window transmission and mirror support obscuration, only about 4% of this energy
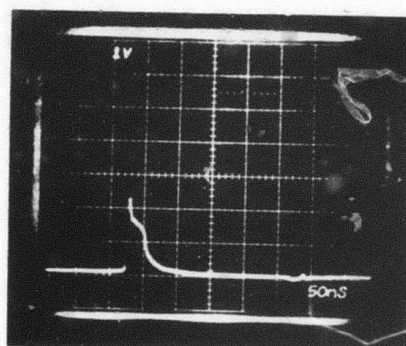
~30 kA/div;
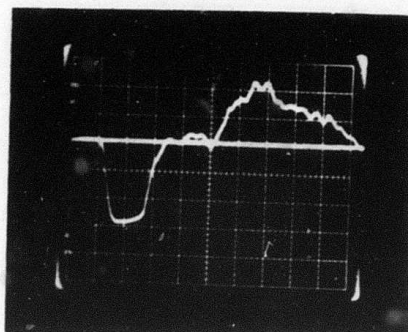
50 ns/div;

(a)

~ 267 MW/div

50 ns/div

(b)

Figure 20.   (a) Electron beam current obtained with a Ḃ pickup
loop located in the beam diode.   Separate shots;
there is not time relation between (a) and (b).
(b) Laser pulse shape obtained by VUV planar
photodiode.   Diode rise time ~ 1 ns, oscilloscope
band width 500 mHz.

which left the laser could be transmitted out of the pressure cell. This is a limitation of the optics, not the laser physics or the excitation scheme. In fact, these experiments show the major problem of constructing high energy/high power vacuum UV lasers is the unavailability of appropriate optical components. Here is where the new technology needs to be developed that will enable further progress in this part of the elctromagnetic spectrum. It was beyond the scope of this program to investigate this interesting and challenging area of research. Perhaps future advances in this area will allow higher energy vacuum UV lasers to be made with the exciting prospect of studying target interactions at these short wavelengths.

4.0 REFERENCES

1. M. J. Berger and S. M. Seltzer, _Studies in Penetration of Charged Particles in Matter_, National Academy of Sciences Publications, No. 1133, Chap. 10, 1967.

2. L. R. Peterson and J. E. Allen, J. Chem. Phys. __56,__ 6068 (1972).

3. J. H. Parks, D. R. Rao and A. Javan, Appl. Phys. Lett. __13,__ 142 (1968).

4. G. Herzberg, _Spectra of Diatomic Molecules_ (D. Van Nostrand Co. Inc., Princeton, 1950).

5. D. E. Shemansky and A. L. Broadfoot, J. Quant, Spectrosc, Radiat. Transfer. __11,__ 1385 (1971).